1 SI

1.1 Methods Figures

This is a selection of Figures to support the discussion of non-linearity and state dependence in the main Methods Section.

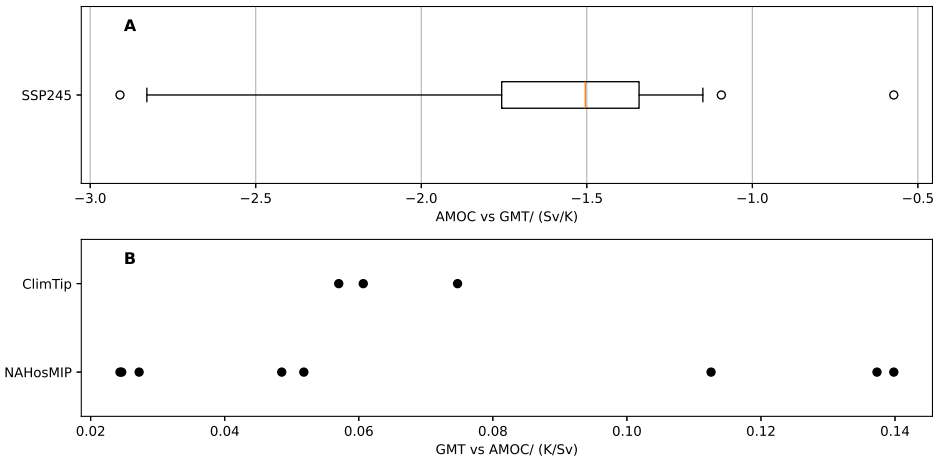


Fig. 1 Calculated regressions of the impact of realised global mean temperature changes on Atlantic meridional overturning circulation in CMIP6 scenarios (α panel A) and of AMOC changes on GMT change in hosing scenarios (β panel B). Boxplots show the median with an orange line, box gives the interquartile range, the tails give the 5th and 95th percentiles, and hollow circles are used for points outside this range. For Panel B, points represent individual model values, as there is significantly less data. The panel A SSP245 analysis includes all 7 of the models used in the main analysis of the paper, the panel B analysis of AMOC impact on GMT uses all runs of models from ClimTip and NAHosMIP to give a larger ensemble size.

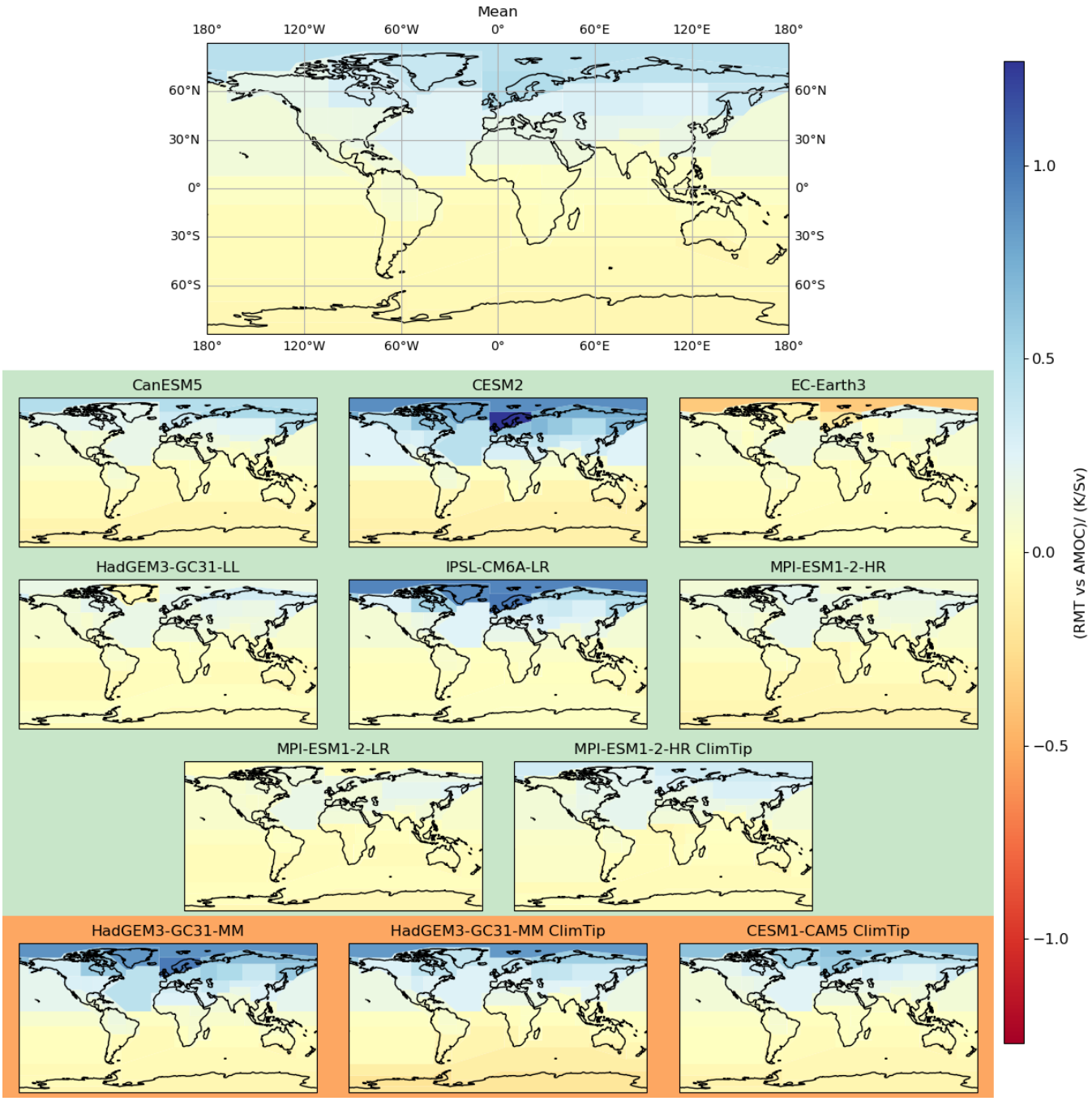


Fig. 2 The regression impacts of AMOC change on regional mean temperature in a range of hosing experiments (lower panels) as well as the multi-model mean (upper panel). The panels highlighted in green are taken from the seven models (with two scenarios for MPI-ESM1-2-HR) utilised in the main analysis, while those in orange are included for comparison and the development of the methodology but are not used in the main analysis. Displays the range of regional mean temperature responses seen across the models, as well as common features such as a cooling Northern Hemisphere, stronger responses around the North Atlantic, and weaker responses in the Southern Hemisphere.

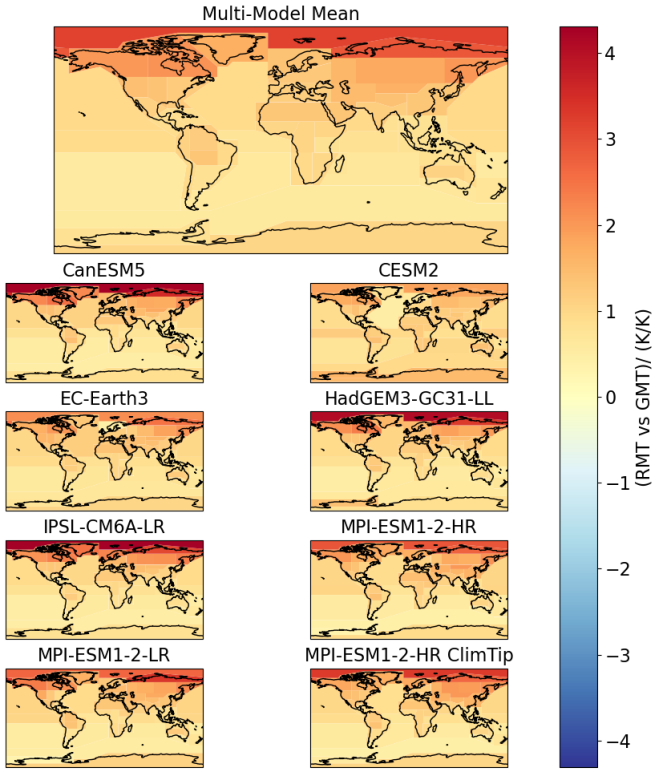


Fig. 3 The regression impacts of greenhouse gas-driven global mean temperature on regional mean temperatures, after adjusting for AMOC change on both variables (Parameter γ in the framework). This should give the relationship in a counterfactual world where AMOC does not change. The expected features are present, with warming seen across the globe, stronger in the polar regions (polar amplification) and over land, with weaker warming over the ocean. The North Atlantic warming hole is not seen strongly here, as might be expected if it is strongly related to AMOC behaviour. Results are presented for each of the 7 models in the main analysis, with two plots for MPI-ESM1-2-HR, one using the NAHosMIP AMOC response and the other the ClimTip response.

1.2 Table of Models

Table of models, variants, and experiments included in the analysis or used for the comparison of AMOC impacts and state dependence

Table 1 Sample Table

Model	SSP245 Variants	Hosing Variants (NAHosMIP unless specified)	Parameters	Reference
CanESM5	r[1-10]i1p[1-2]f1	r1i1p2f1	α,β,γ,δ	Swart et al. [1]
CESM1-CAM5		r1i1p1f1 (ClimTip)	β,δ	Hurrell et al. [2]
CESM2	r4i1p1f1	r1i1p2f1	α,β,γ,δ	Danabasoglu et al. [3]
EC-Earth3	r1i1p1f1	r1i1p1f1	α,β,γ,δ	Döscher et al. [4]
HadGEM3-GC31-LL	r[1-4]i1p1f3	r1i1p1f1	α,β,γ,δ	Williams et al. [5]
HadGEM3-GC31-MM		r1i1p1f1, r1i1p1f1 (ClimTip)	β,δ	Williams et al. [5]
IPSL-CM6A-LR	r[1-3]i1p1f1	r1i1p1f1	α,β,γ,δ	Boucher et al. [6]
MPI-ESM1-2-HR	r1i1p1f1	r1i1p1f1	α,β,γ,δ	Müller et al. [7]
MPI-ESM1-2-LR	r[1-3]i1p1f1	r1i1p1f1, r1i1p1f1 (ClimTip)	α,β,γ,δ	Mauritsen et al. [8]

1.3 Regression Figures

Figures demonstrating how the parameters in the framework were derived for each of the models in the analysis, as in Figure 2 for the CanESM5 model.

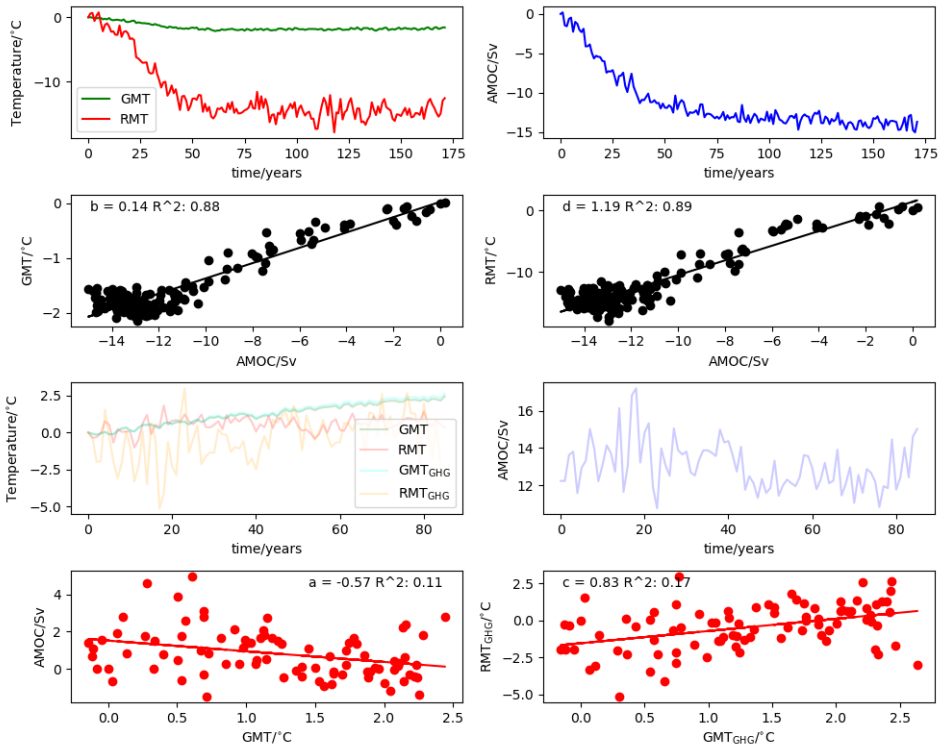


Fig. 4 CESM2 Figure regression figure as in Figure 2

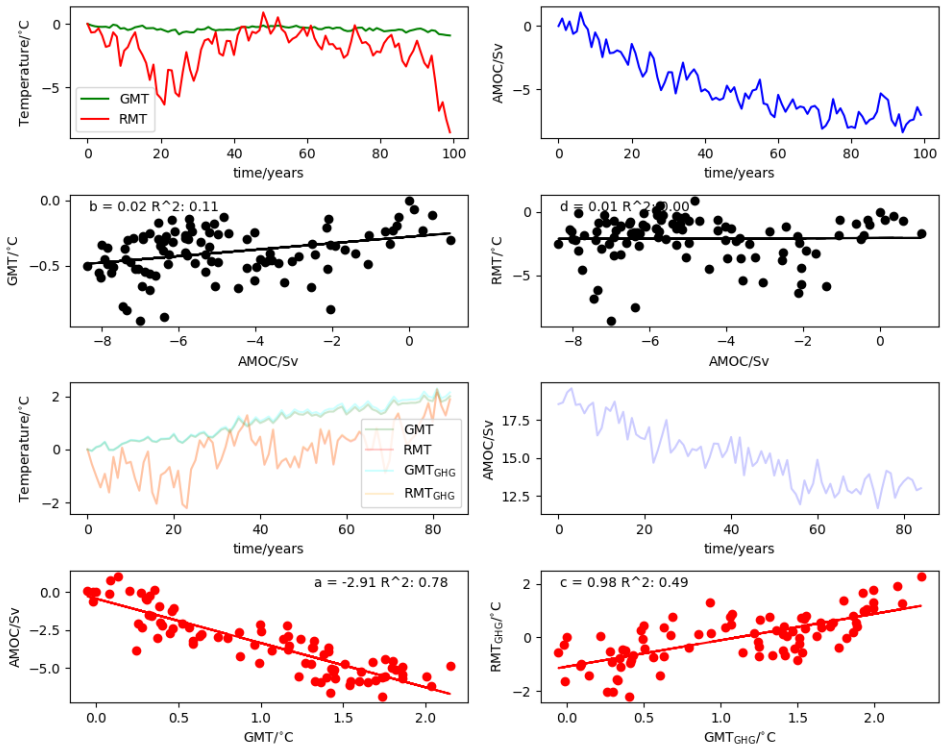


Fig. 5 EC-Earth3 Figure regression figure as in Figure 2

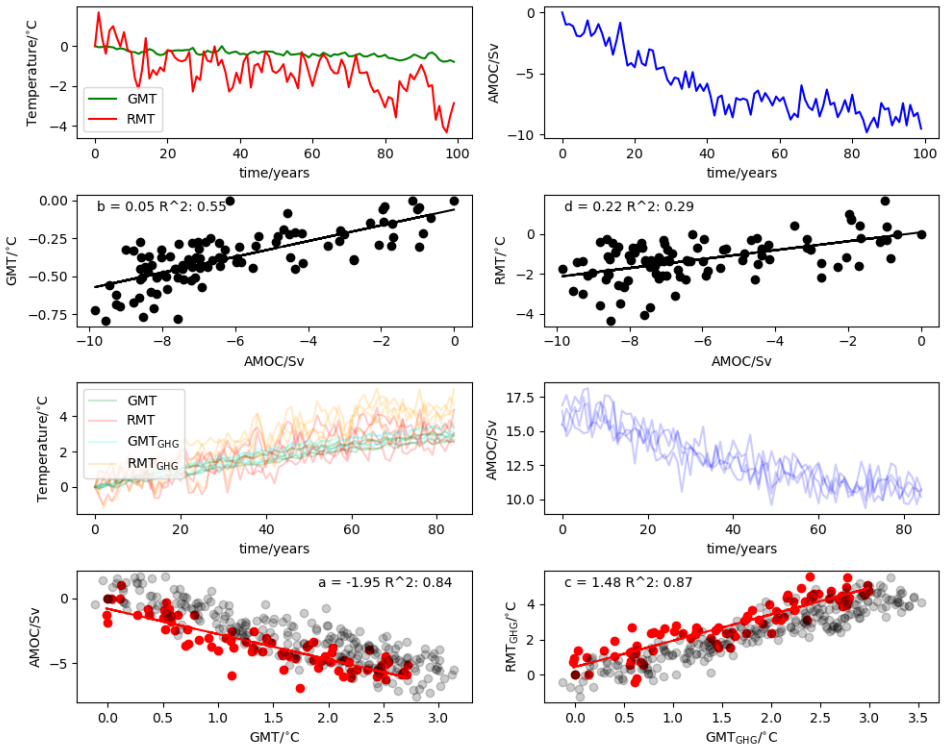


Fig. 6 HadGEM3-GC31-LL Figure regression figure as in Figure 2

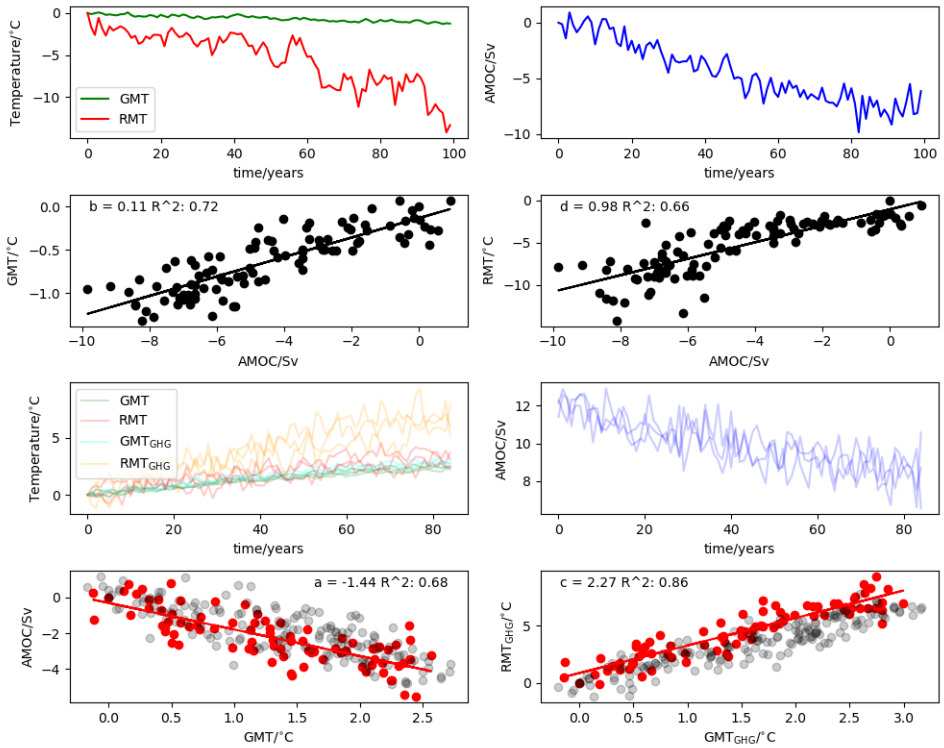


Fig. 7 IPSL-CM6A-LR Figure regression figure as in Figure 2

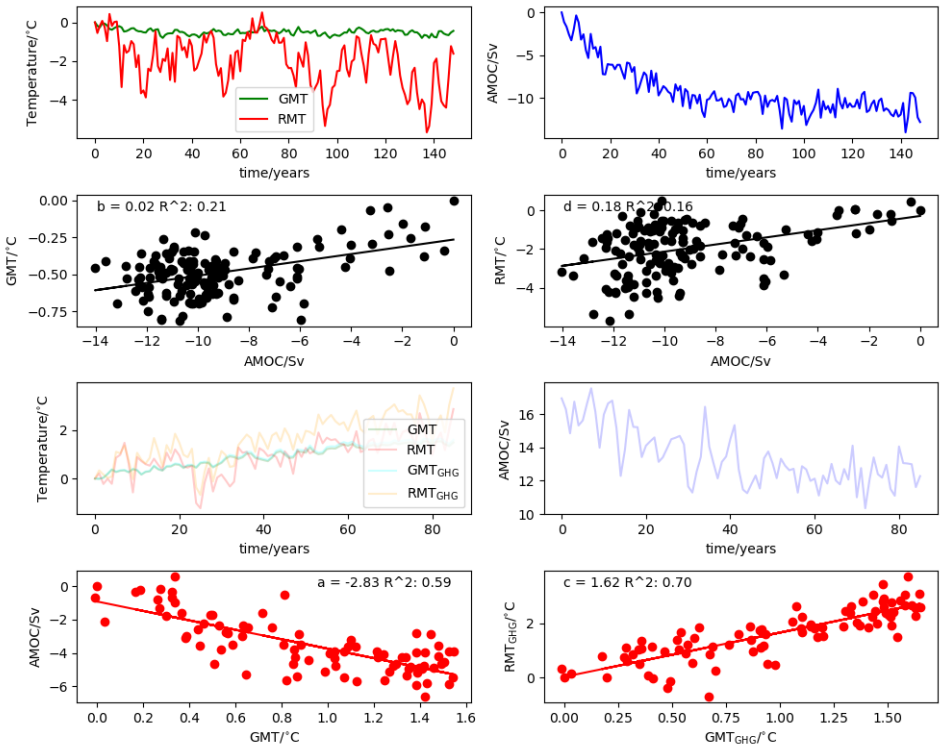


Fig. 8 MPI-ESM1-2-HR Figure regression figure as in Figure 2

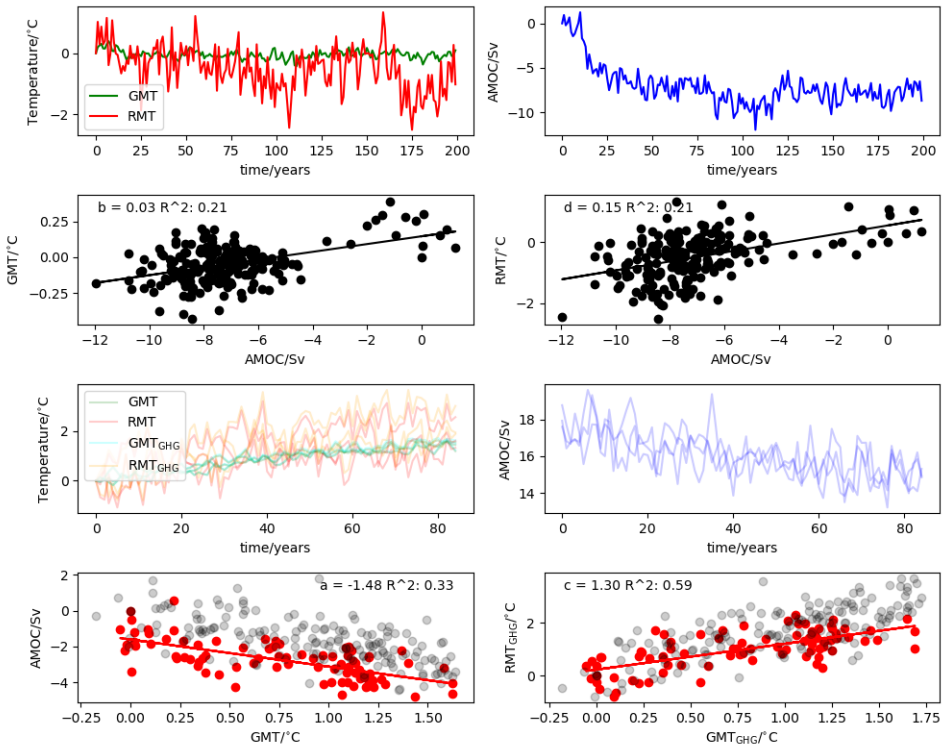


Fig. 9 MPI-ESM1-2-LR Figure regression figure as in Figure 2

1.4 Parameter Correlations

Correlation plots for the parameters across the multi-model ensemble (each dot representing the mean parameter value for a given model). Strong correlations are seen between α and β, α and δ, and β and δ. However, the correlation between β and δ is by far the strongest with a correlation coefficient of 0.99, suggesting these two parameters should be considered jointly.

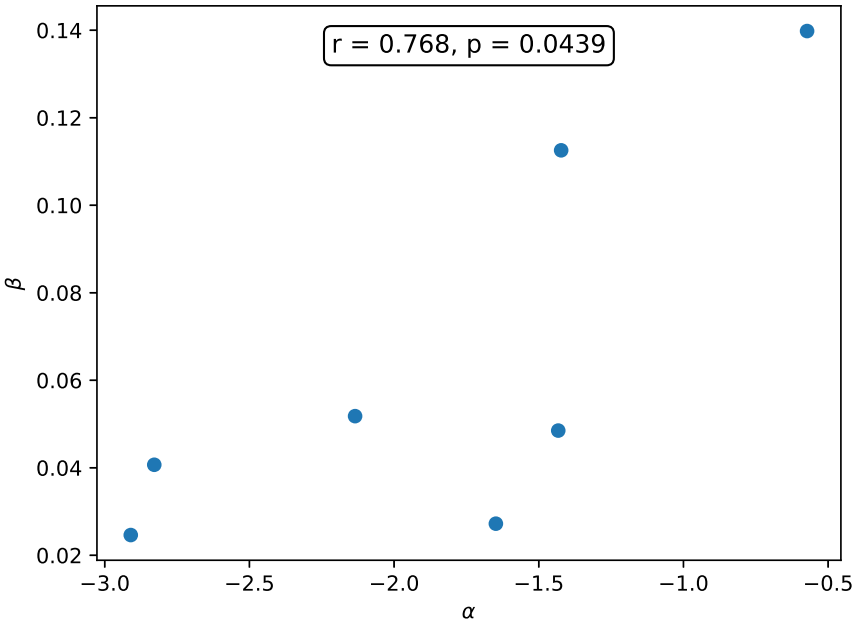


Fig. 10 Scatter plot of parameter values for α and β, each dot represents the mean parameters calculated from runs of a single model. The correlation coefficient and associated p-value are given in the corner of the figure.

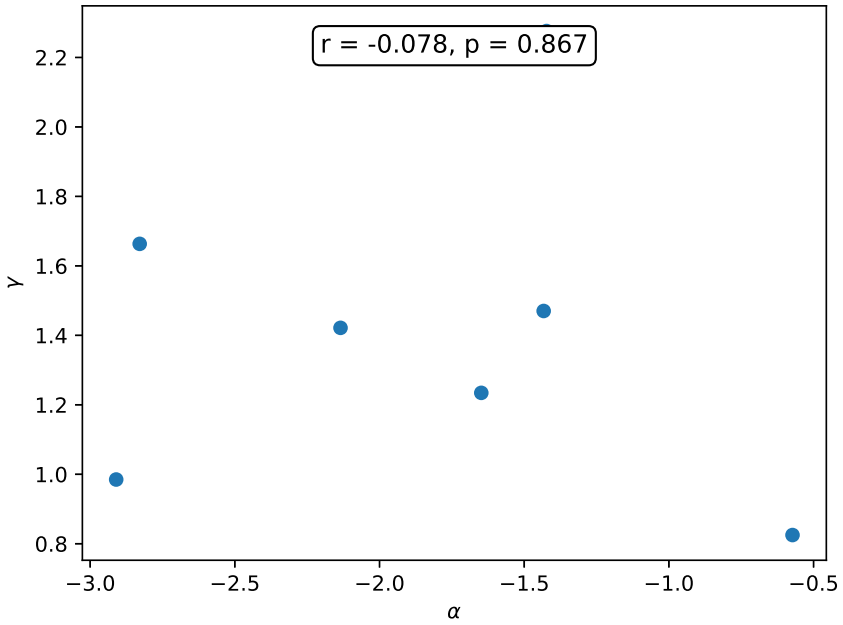


Fig. 11 Scatter plot of parameter values for α and γ, each dot represents the mean parameters calculated from runs of a single model. The correlation coefficient and associated p-value are given in the corner of the figure. γ is calculated for Northern Europe.

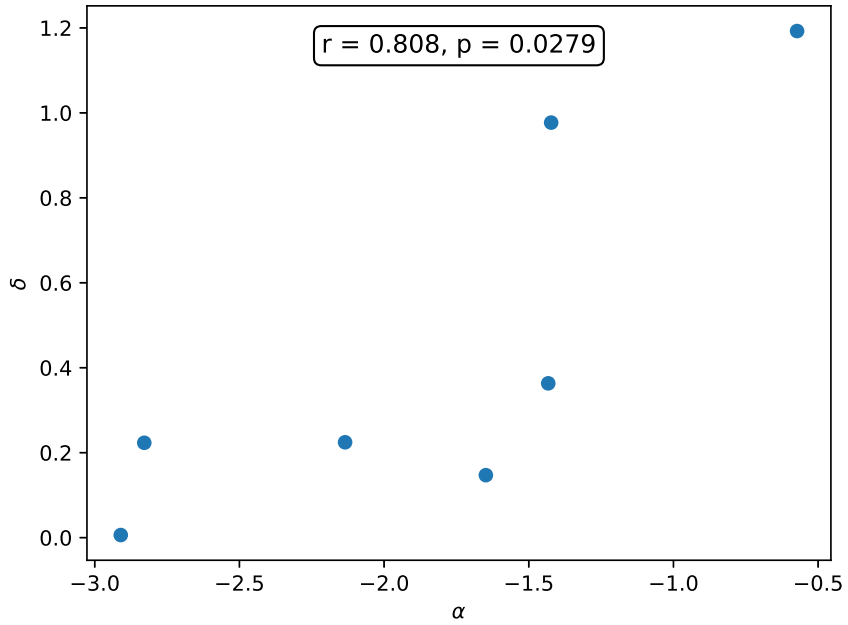


Fig. 12 Scatter plot of parameter values for α and δ, each dot represents the mean parameters calculated from runs of a single model. The correlation coefficient and associated p-value are given in the corner of the figure. δ is calculated for Northern Europe.

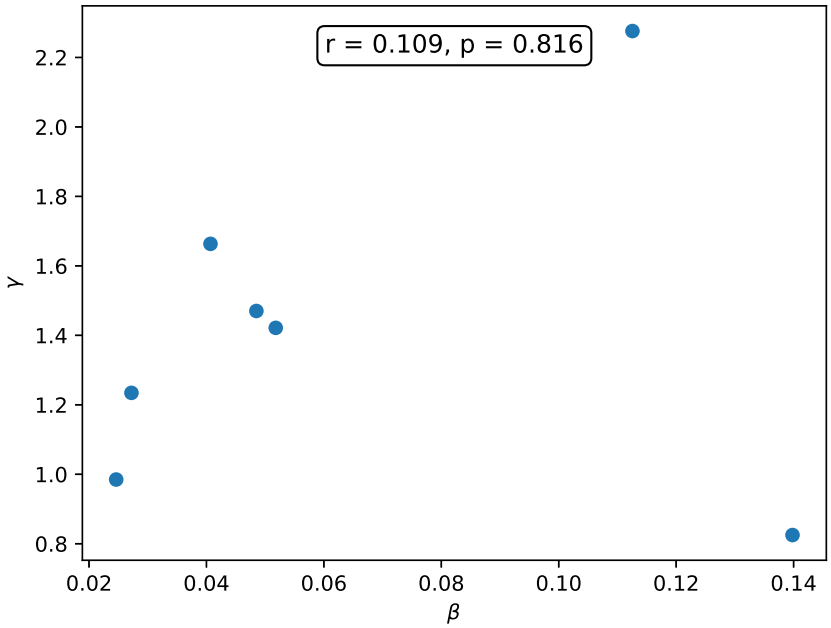


Fig. 13 Scatter plot of parameter values for β and γ, each dot represents the mean parameters calculated from runs of a single model. The correlation coefficient and associated p-value are given in the corner of the figure. γ is calculated for Northern Europe.

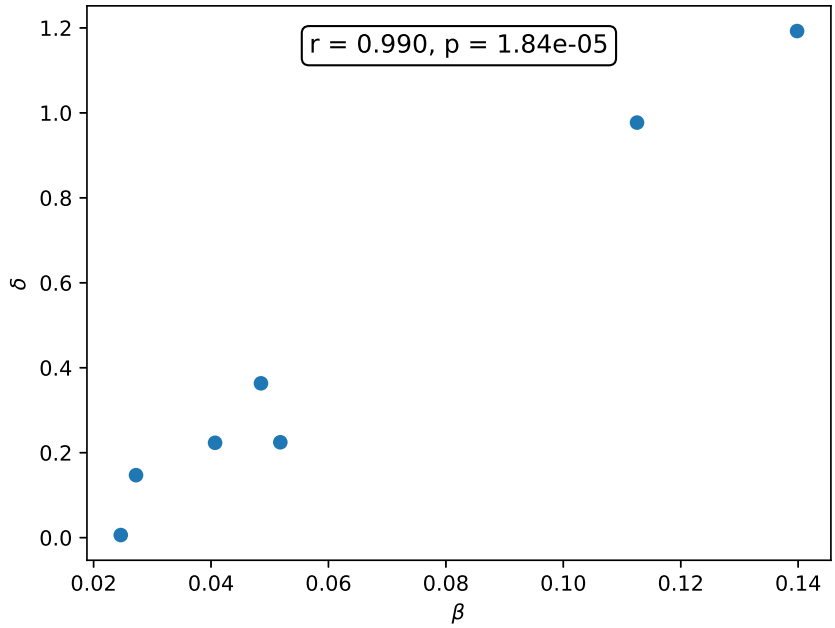


Fig. 14 Scatter plot of parameter values for β and δ, each dot represents the mean parameters calculated from runs of a single model. The correlation coefficient and associated p-value are given in the corner of the figure. δ is calculated for Northern Europe.

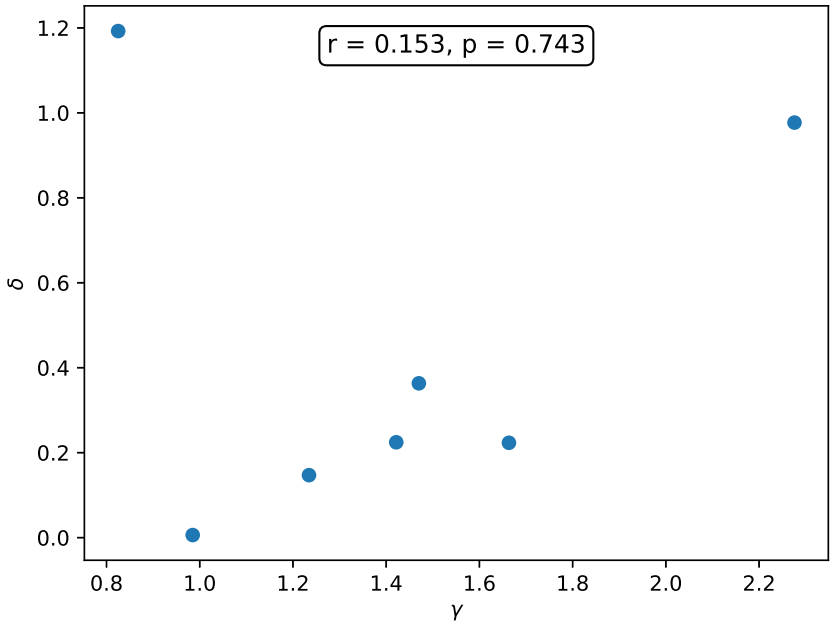


Fig. 15 Scatter plot of parameter values for γ and δ, each dot represents the mean parameters calculated from runs of a single model. The correlation coefficient and associated p-value are given in the corner of the figure. γ and δ are calculated for Northern Europe.

1.5 Regional Temperature Impacts

Regional temperature projections for IPCC AR6 regions other than Northern Europe, using the framework as in Figure 3, for a 12 Sv decline by 2100 under an SSP245 scenario.

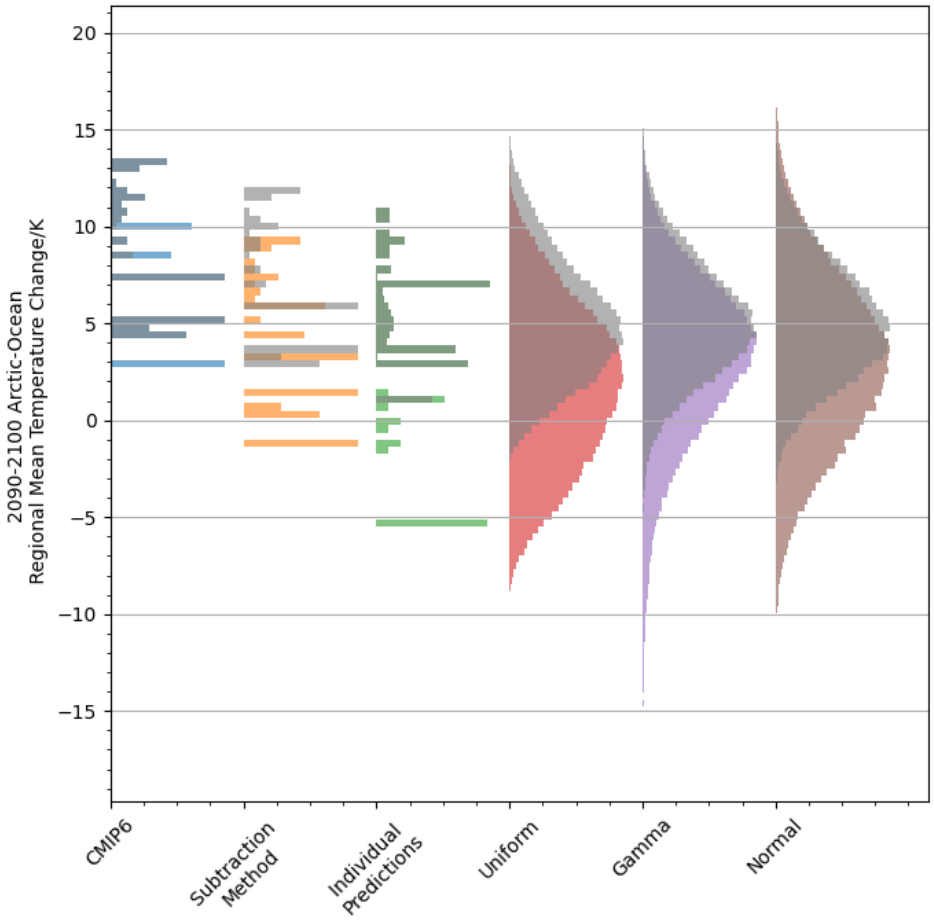


Fig. 16 Histograms of the 2090-2100 regional mean temperature in the CMIP SSP245 runs and the large AMOC decline scenario (-12Sv) for the Arctic Ocean as in Figure 3

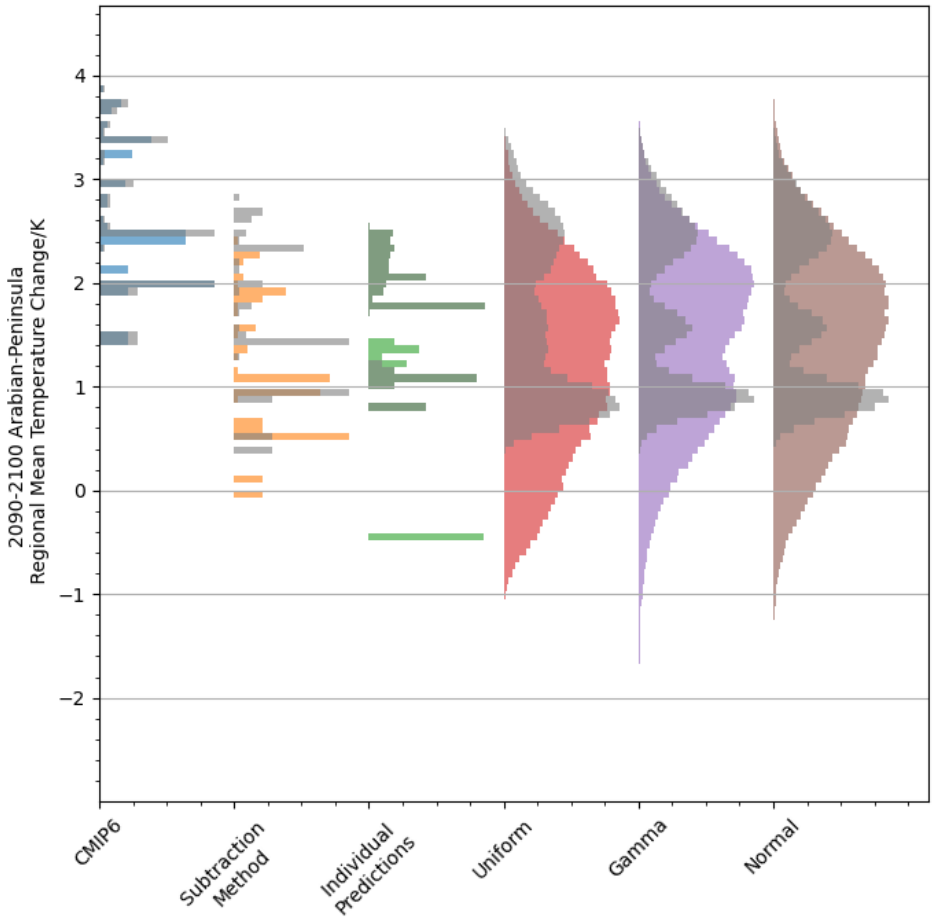


Fig. 17 Histograms of the 2090-2100 regional mean temperature in the CMIP SSP245 runs and the large AMOC decline scenario (-12Sv) for the Arabian Peninsula as in Figure 3

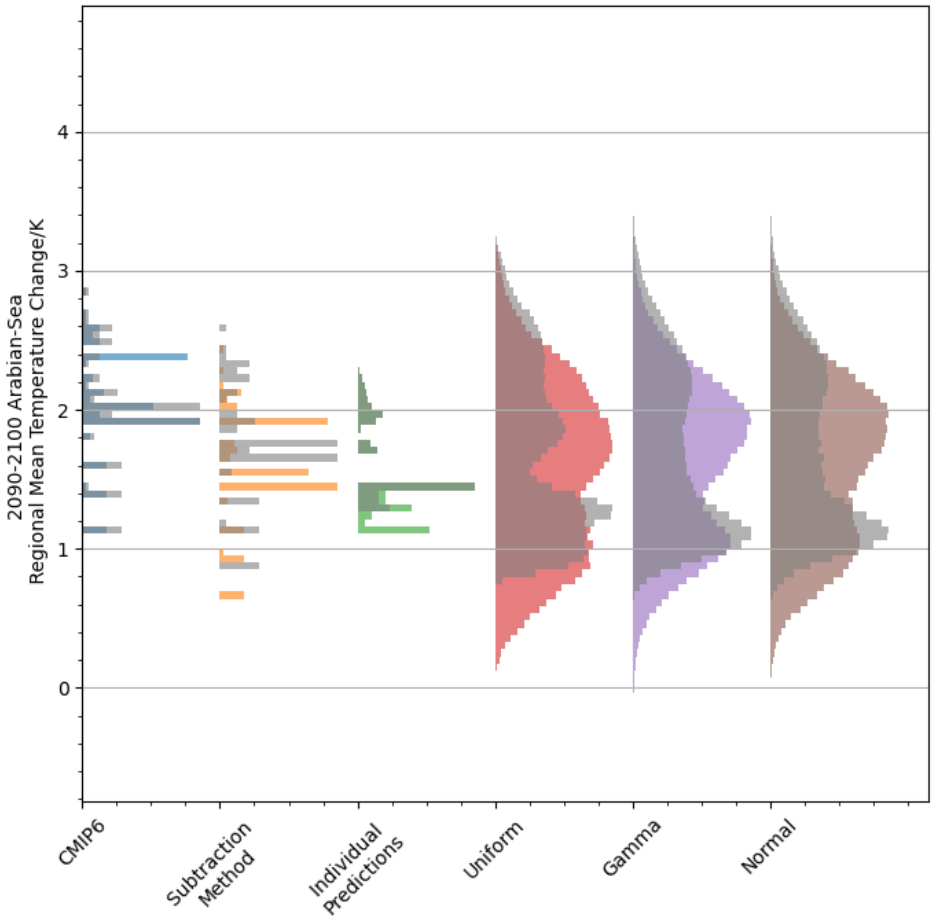


Fig. 18 Histograms of the 2090-2100 regional mean temperature in the CMIP SSP245 runs and the large AMOC decline scenario (-12Sv) for the Arabian Sea as in Figure 3

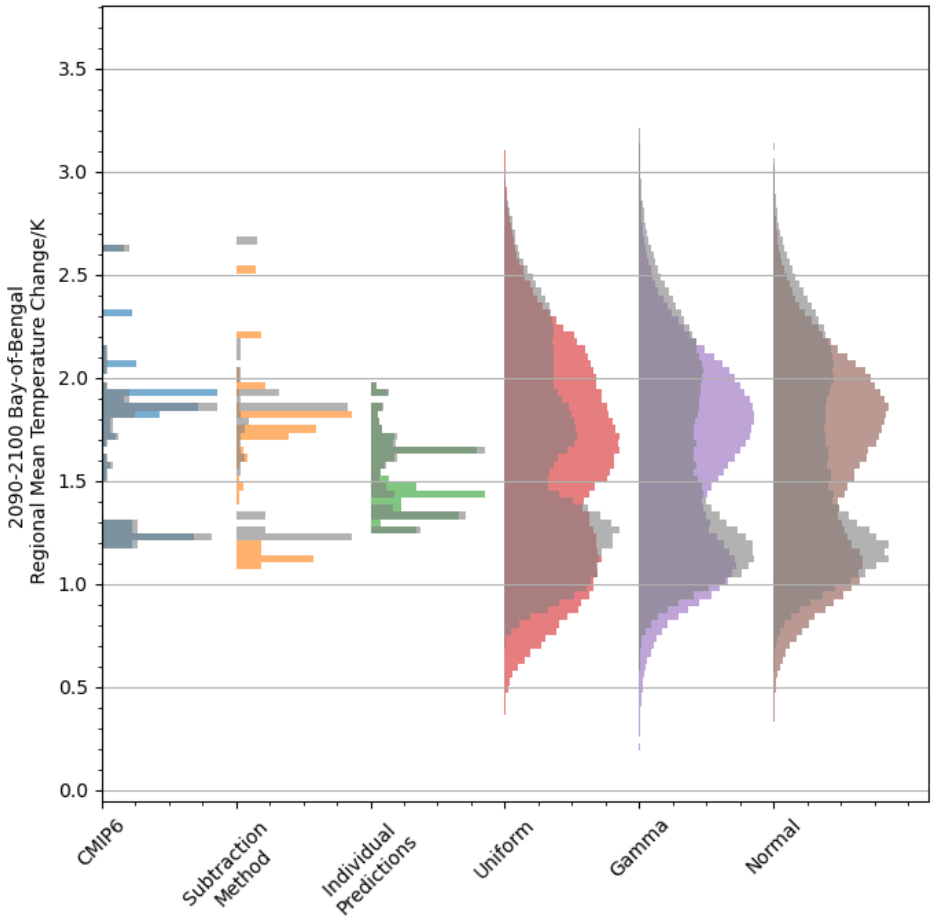


Fig. 19 Histograms of the 2090-2100 regional mean temperature in the CMIP SSP245 runs and the large AMOC decline scenario (-12Sv) for the Bay of Bengal as in Figure 3

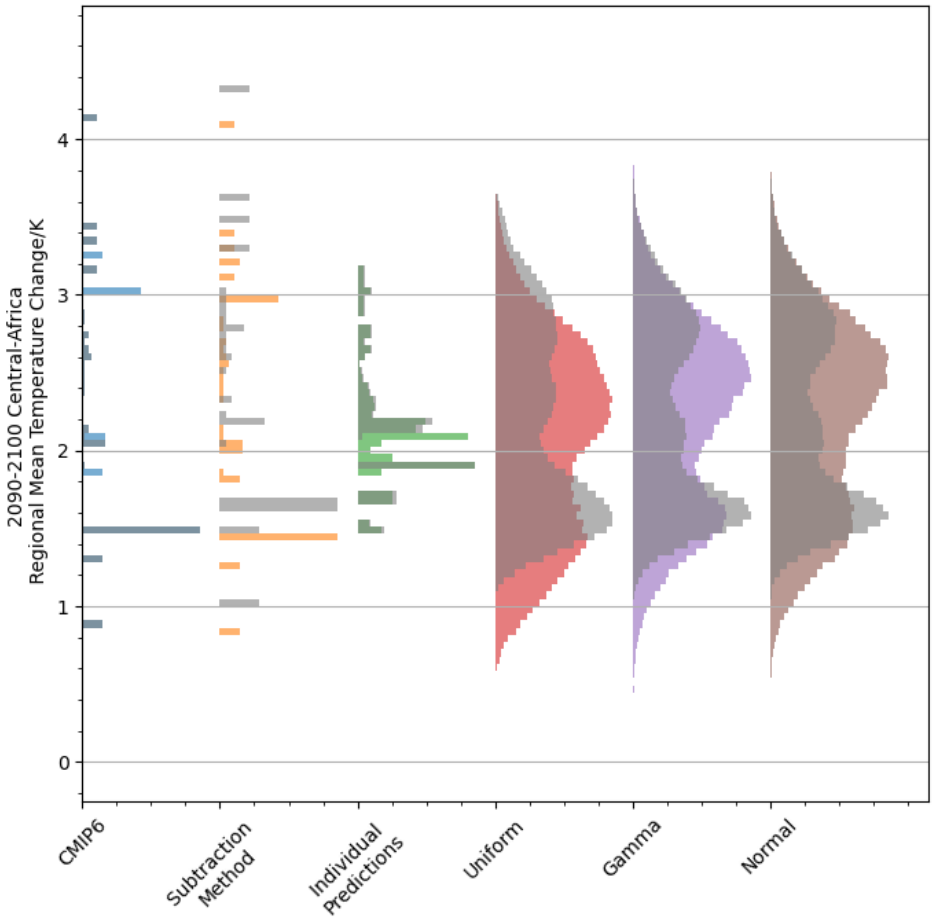


Fig. 20 Histograms of the 2090-2100 regional mean temperature in the CMIP SSP245 runs and the large AMOC decline scenario (-12Sv) for Central Africa as in Figure 3

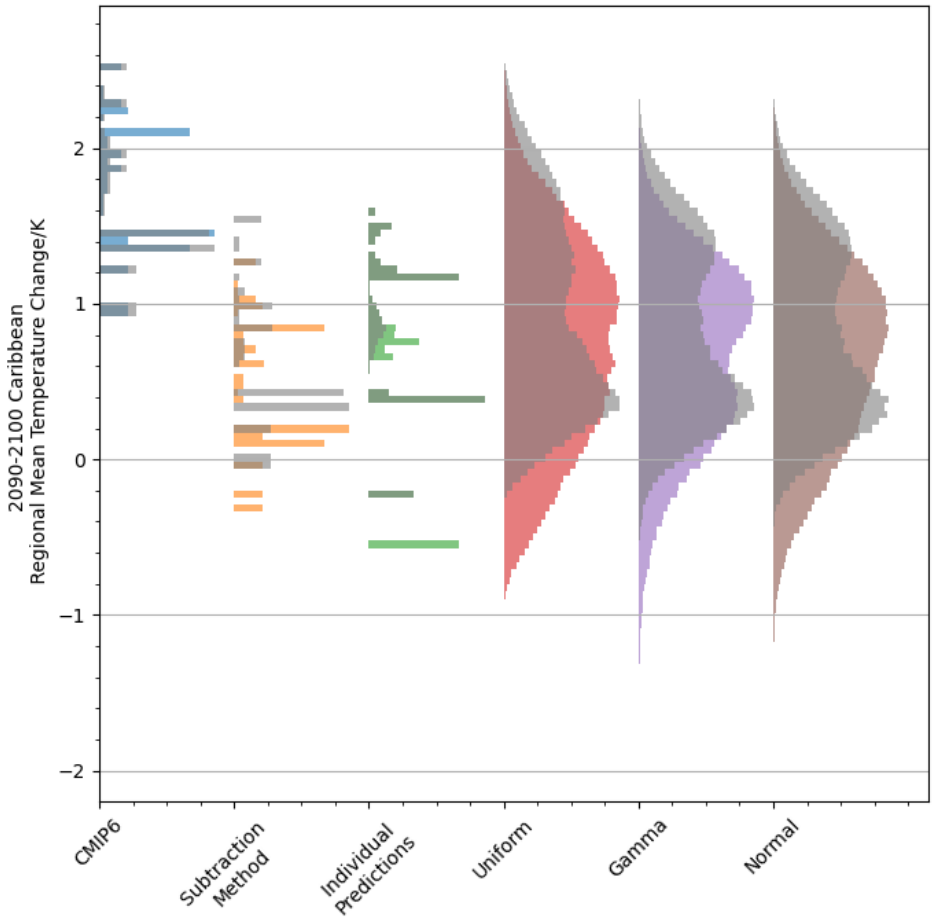


Fig. 21 Histograms of the 2090-2100 regional mean temperature in the CMIP SSP245 runs and the large AMOC decline scenario (-12Sv) for the Caribbean as in Figure 3

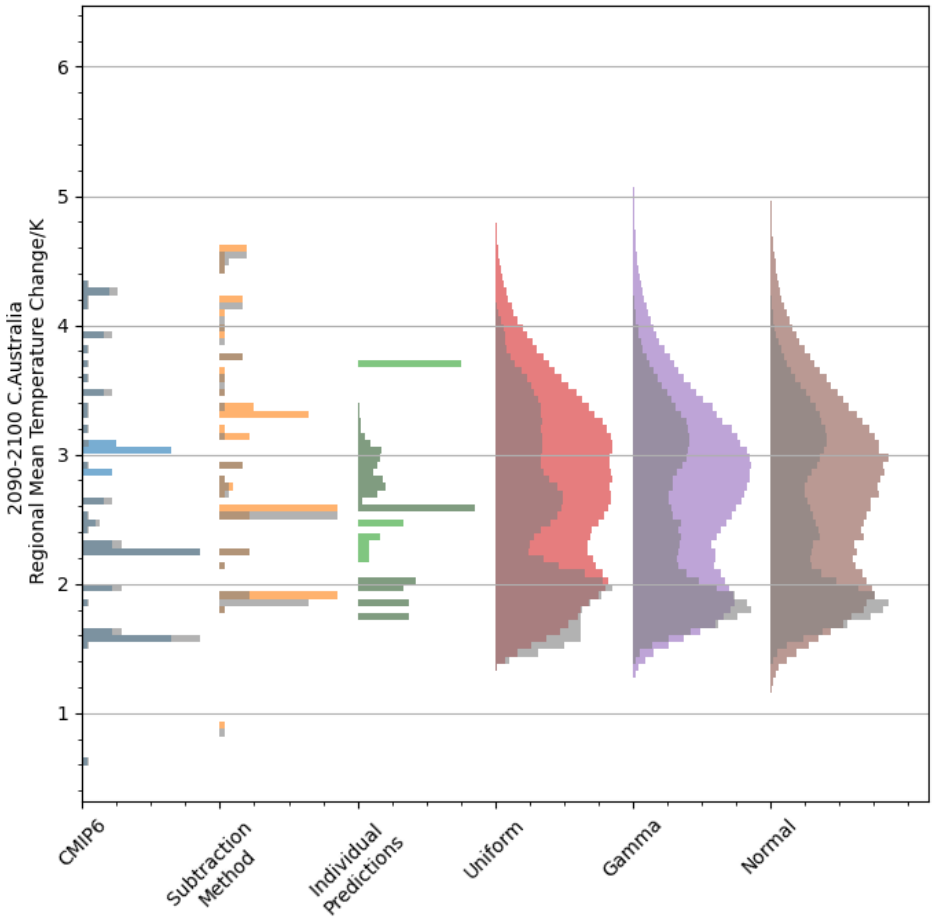


Fig. 22 Histograms of the 2090-2100 regional mean temperature in the CMIP SSP245 runs and the large AMOC decline scenario (-12Sv) for Central Australia as in Figure 3

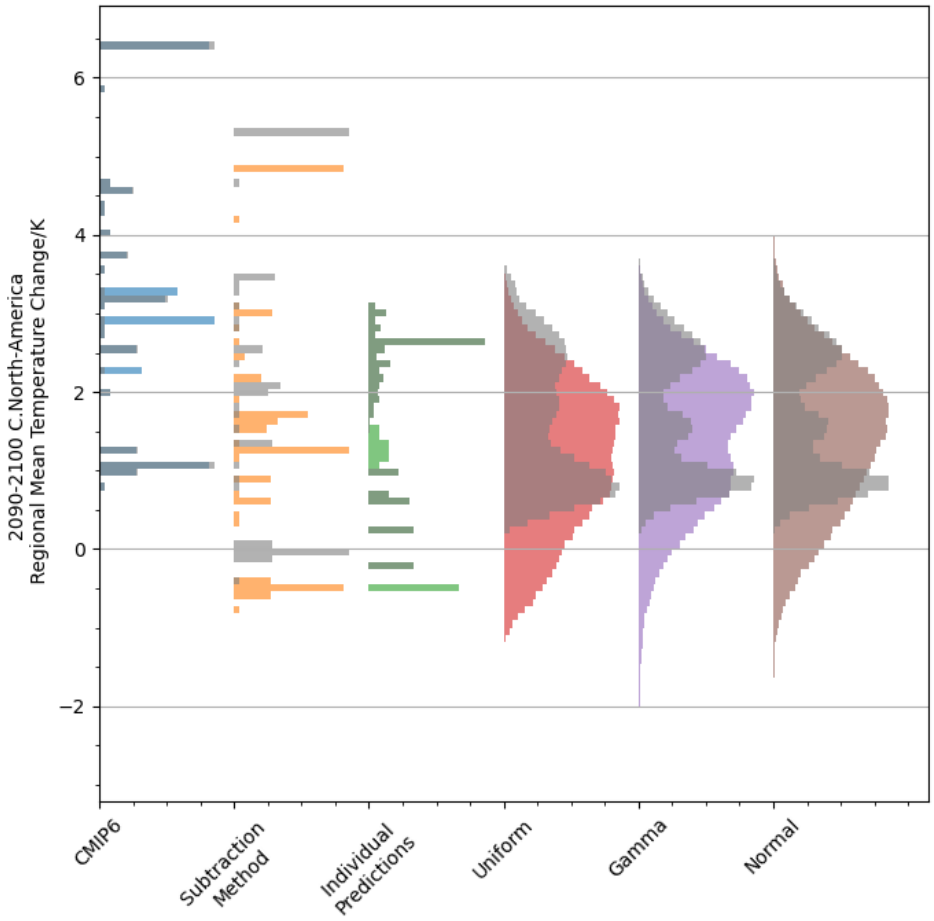


Fig. 23 Histograms of the 2090-2100 regional mean temperature in the CMIP SSP245 runs and the large AMOC decline scenario (-12Sv) for Central North America as in Figure 3

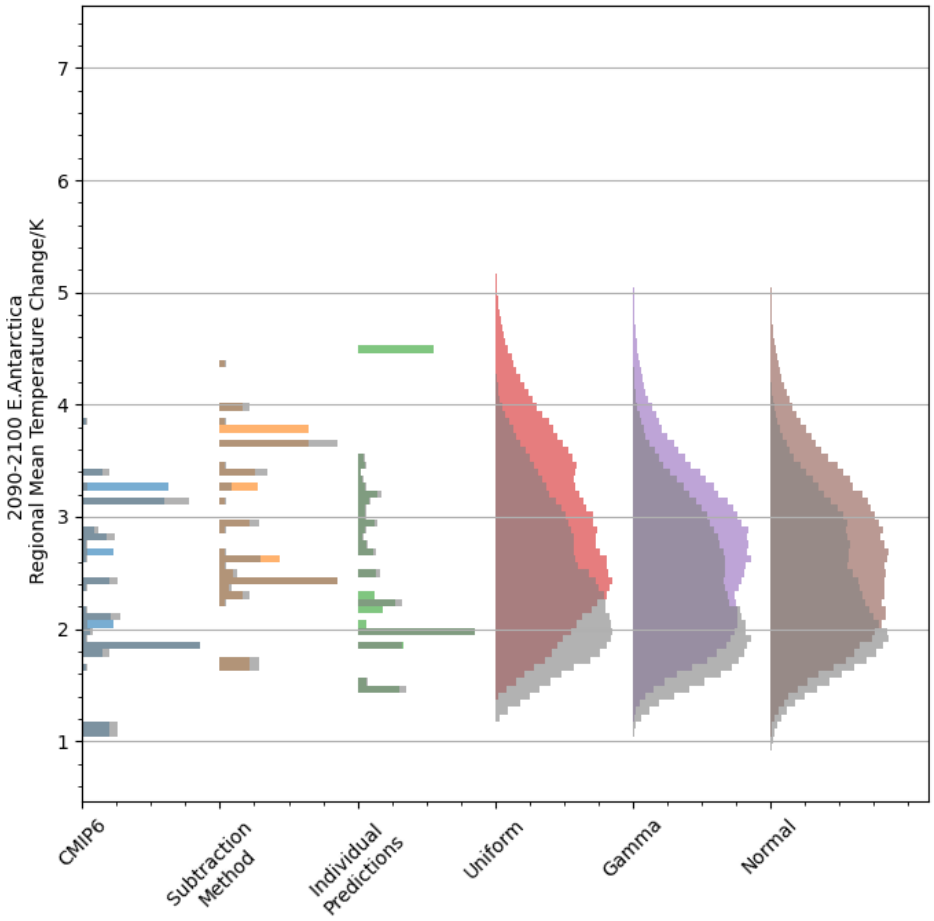


Fig. 24 Histograms of the 2090-2100 regional mean temperature in the CMIP SSP245 runs and the large AMOC decline scenario (-12Sv) for East Antarctica as in Figure 3

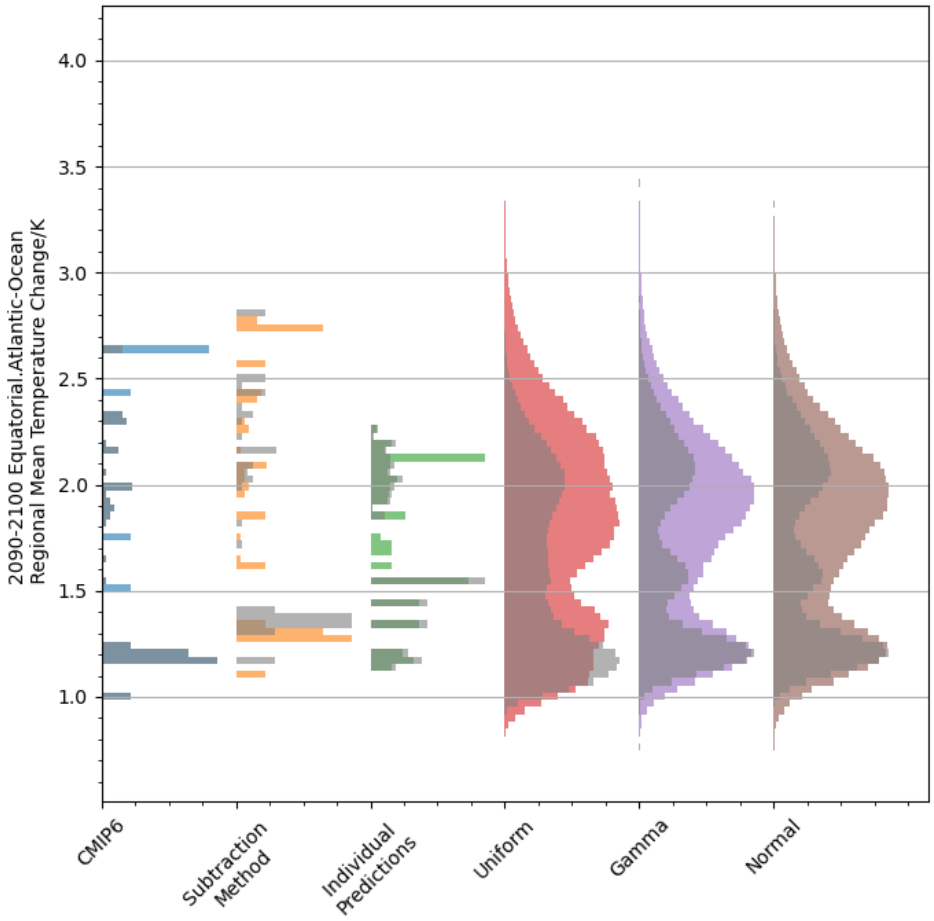


Fig. 25 Histograms of the 2090-2100 regional mean temperature in the CMIP SSP245 runs and the large AMOC decline scenario (-12Sv) for the Equatorial Atlantic Ocean as in Figure 3

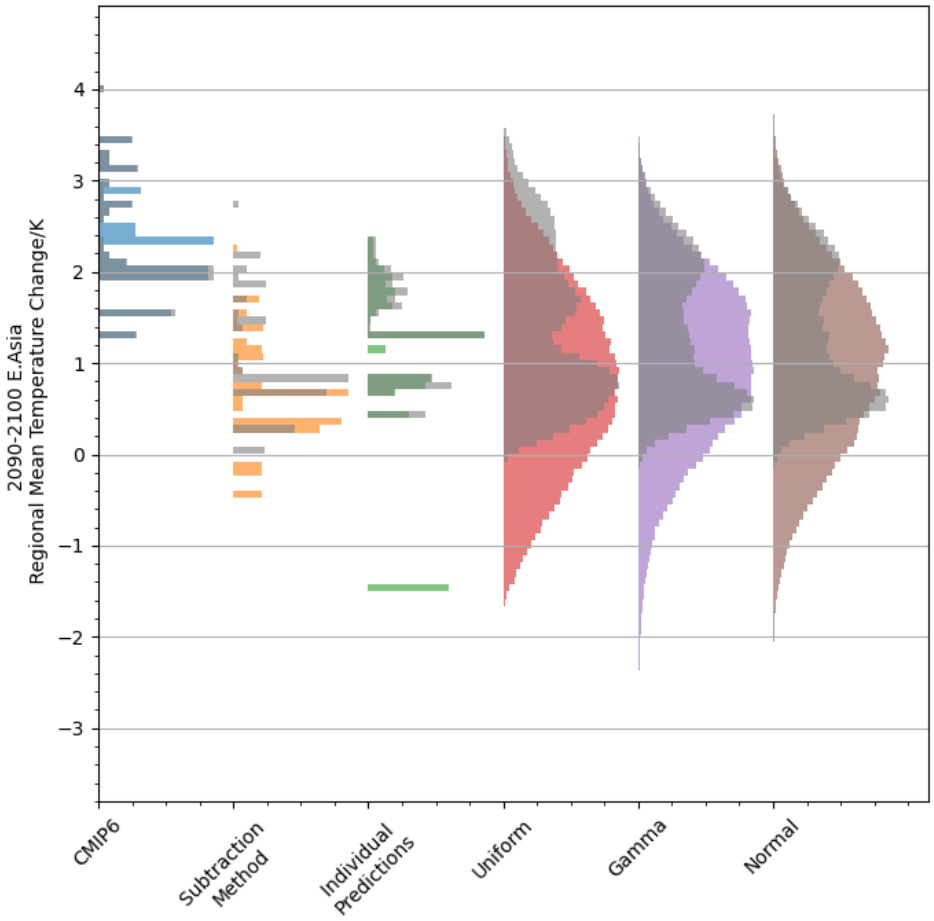


Fig. 26 Histograms of the 2090-2100 regional mean temperature in the CMIP SSP245 runs and the large AMOC decline scenario (-12Sv) for East Asia as in Figure 3

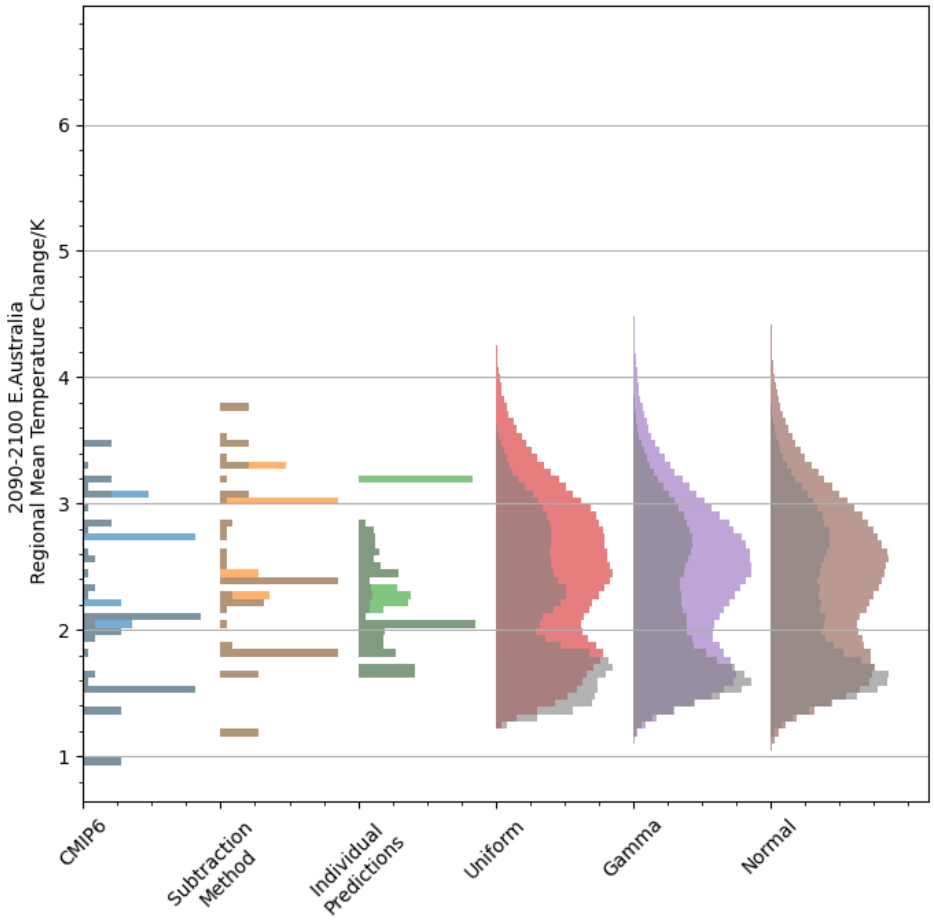


Fig. 27 Histograms of the 2090-2100 regional mean temperature in the CMIP SSP245 runs and the large AMOC decline scenario (-12Sv) for East Australia as in Figure 3

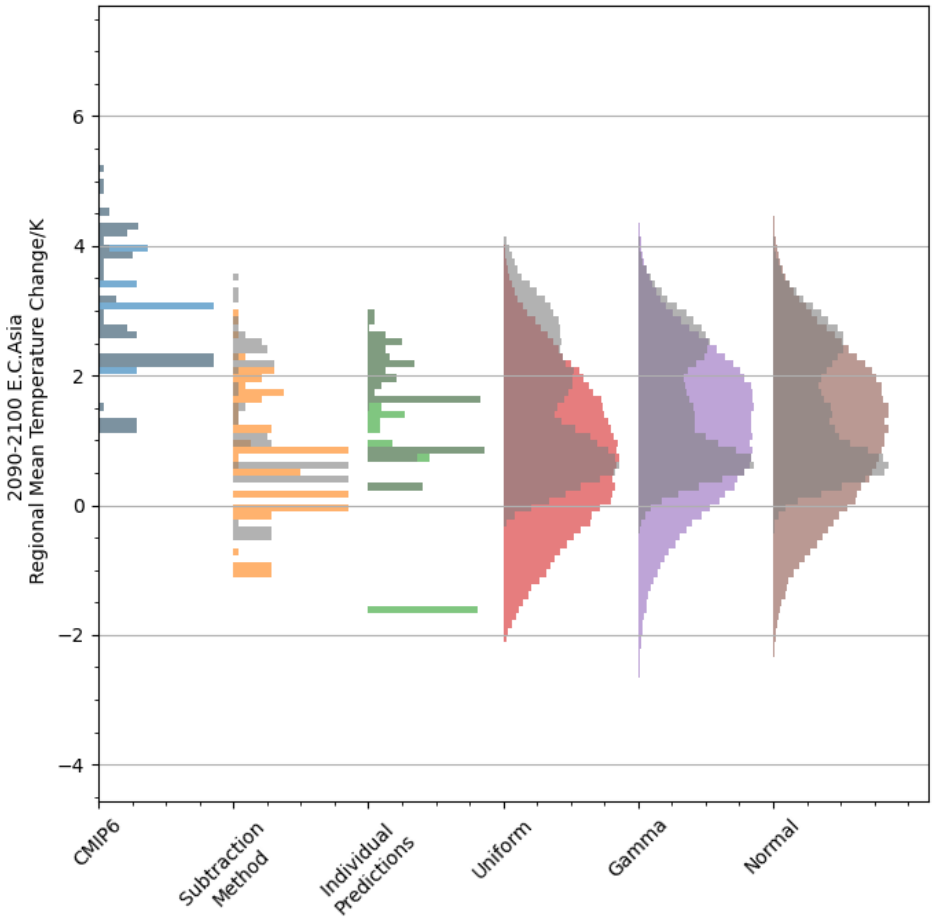


Fig. 28 Histograms of the 2090-2100 regional mean temperature in the CMIP SSP245 runs and the large AMOC decline scenario (-12Sv) for East Central Asia as in Figure 3

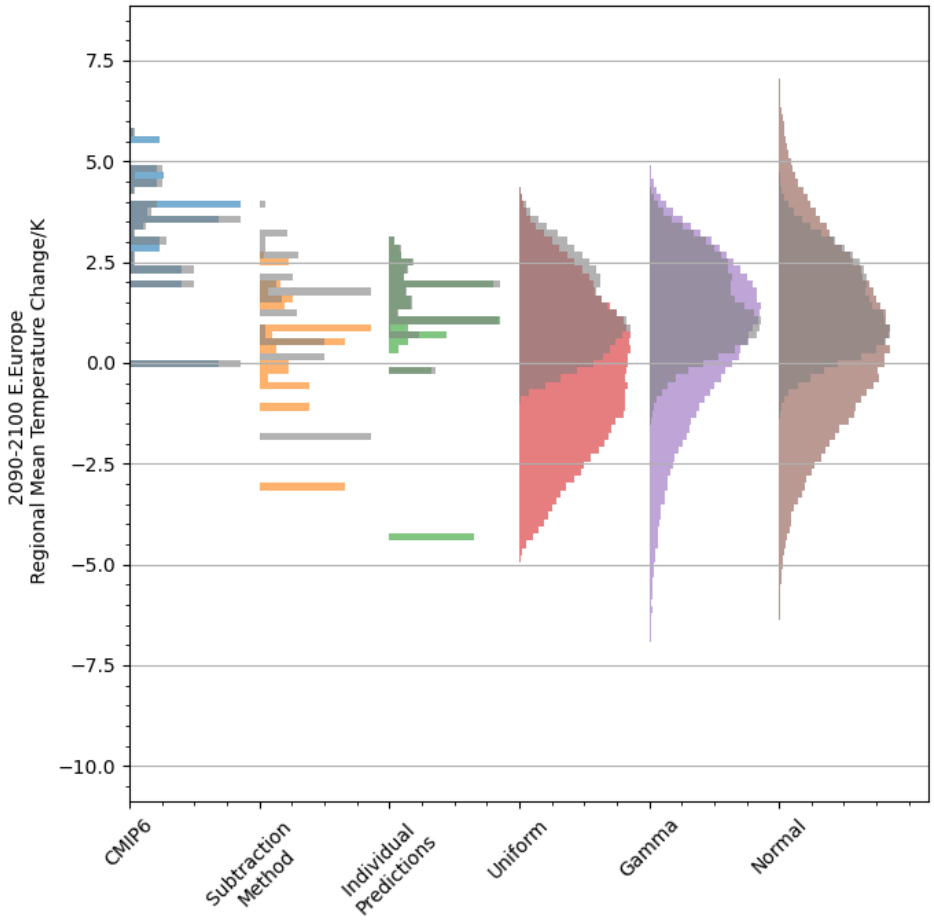


Fig. 29 Histograms of the 2090-2100 regional mean temperature in the CMIP SSP245 runs and the large AMOC decline scenario (-12Sv) for Eastern Europe as in Figure 3

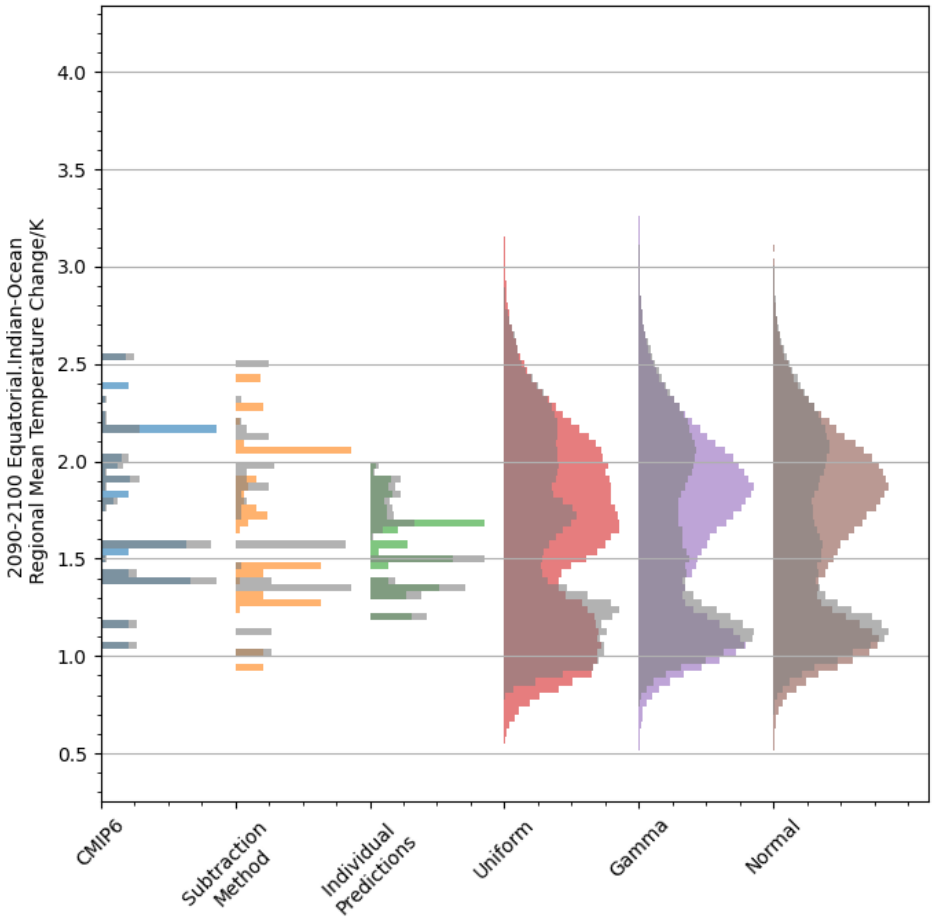


Fig. 30 Histograms of the 2090-2100 regional mean temperature in the CMIP SSP245 runs and the large AMOC decline scenario (-12Sv) for the Equatorial Indian Ocean as in Figure 3

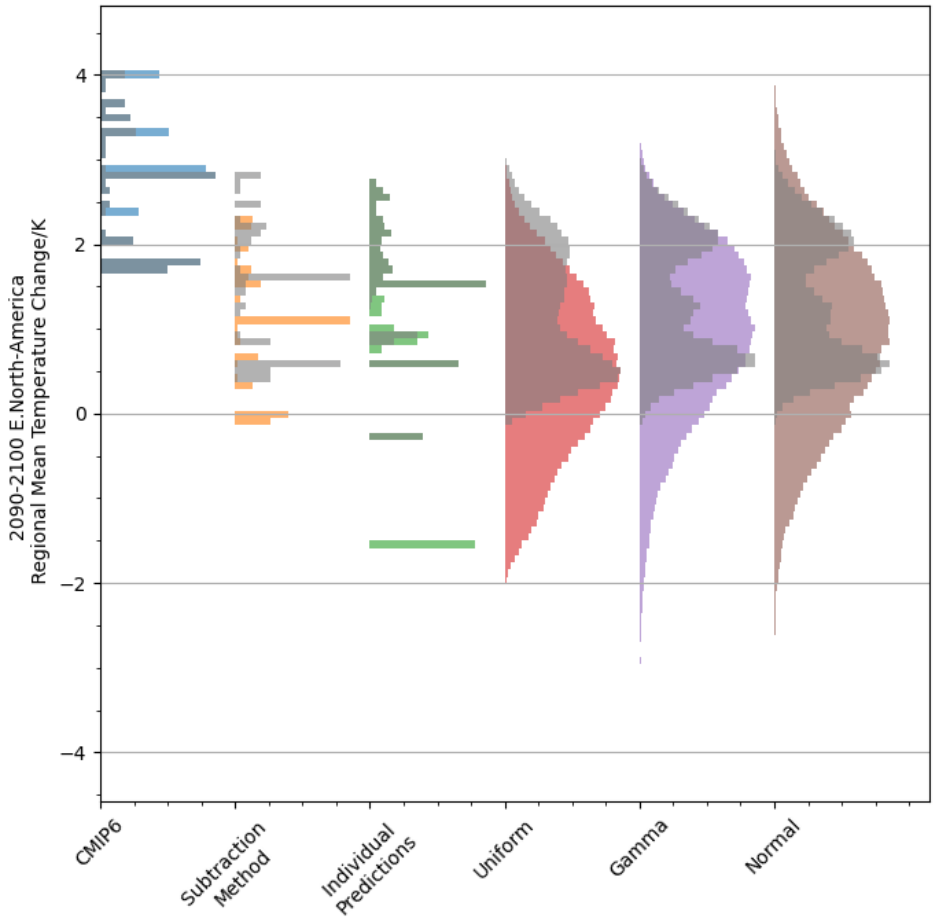


Fig. 31 Histograms of the 2090-2100 regional mean temperature in the CMIP SSP245 runs and the large AMOC decline scenario (-12Sv) for Eastern North America as in Figure 3

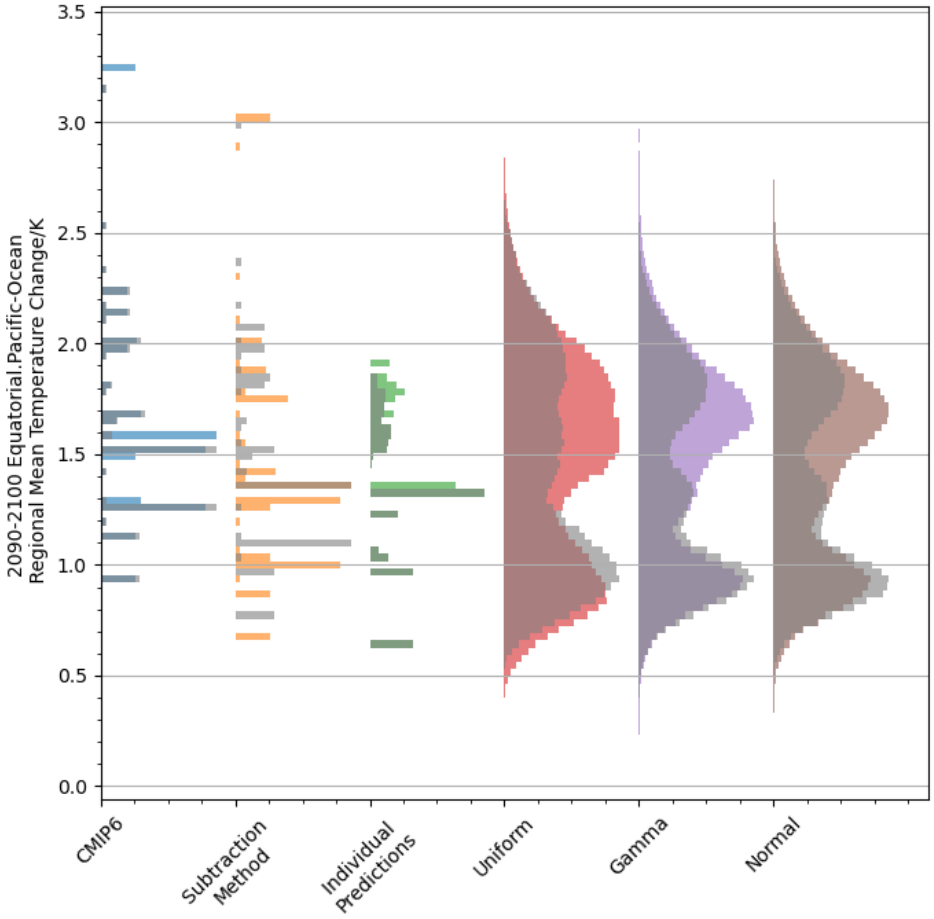


Fig. 32 Histograms of the 2090-2100 regional mean temperature in the CMIP SSP245 runs and the large AMOC decline scenario (-12Sv) for Equatorial Pacific Ocean as in Figure 3

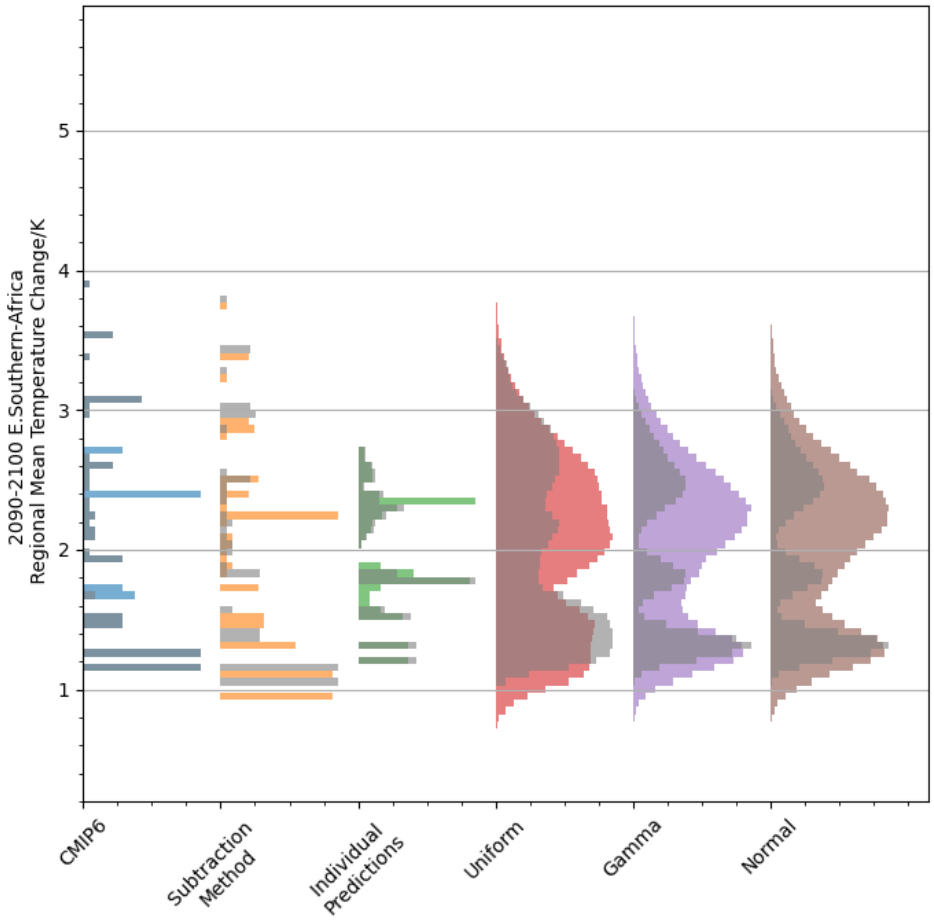


Fig. 33 Histograms of the 2090-2100 regional mean temperature in the CMIP SSP245 runs and the large AMOC decline scenario (-12Sv) for East Southern Africa as in Figure 3

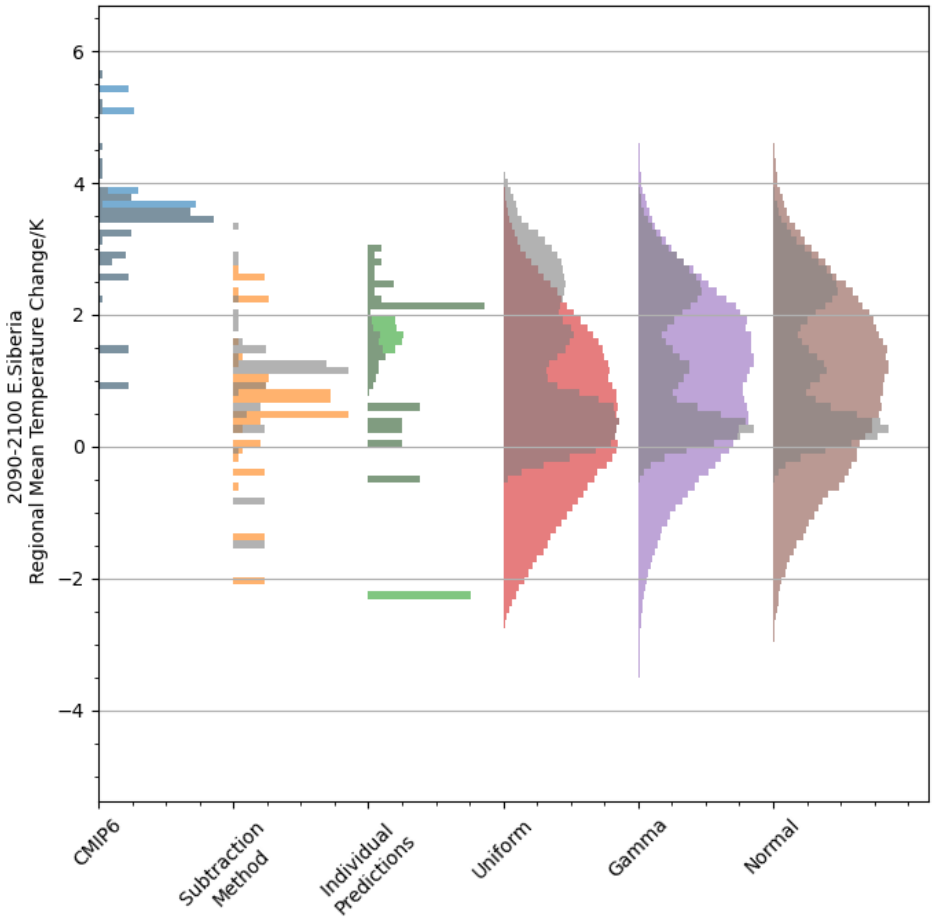


Fig. 34 Histograms of the 2090-2100 regional mean temperature in the CMIP SSP245 runs and the large AMOC decline scenario (-12Sv) for East Siberia as in Figure 3

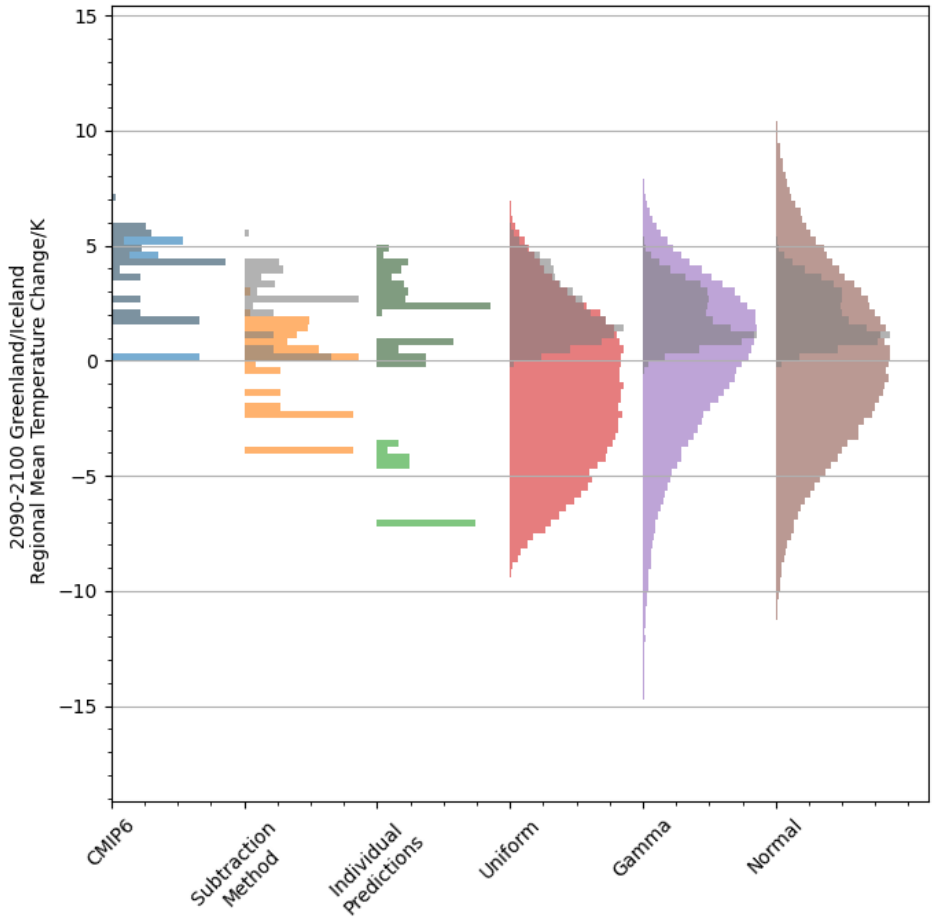


Fig. 35 Histograms of the 2090-2100 regional mean temperature in the CMIP SSP245 runs and the large AMOC decline scenario (-12Sv) for the Greenland Iceland Region as in Figure 3

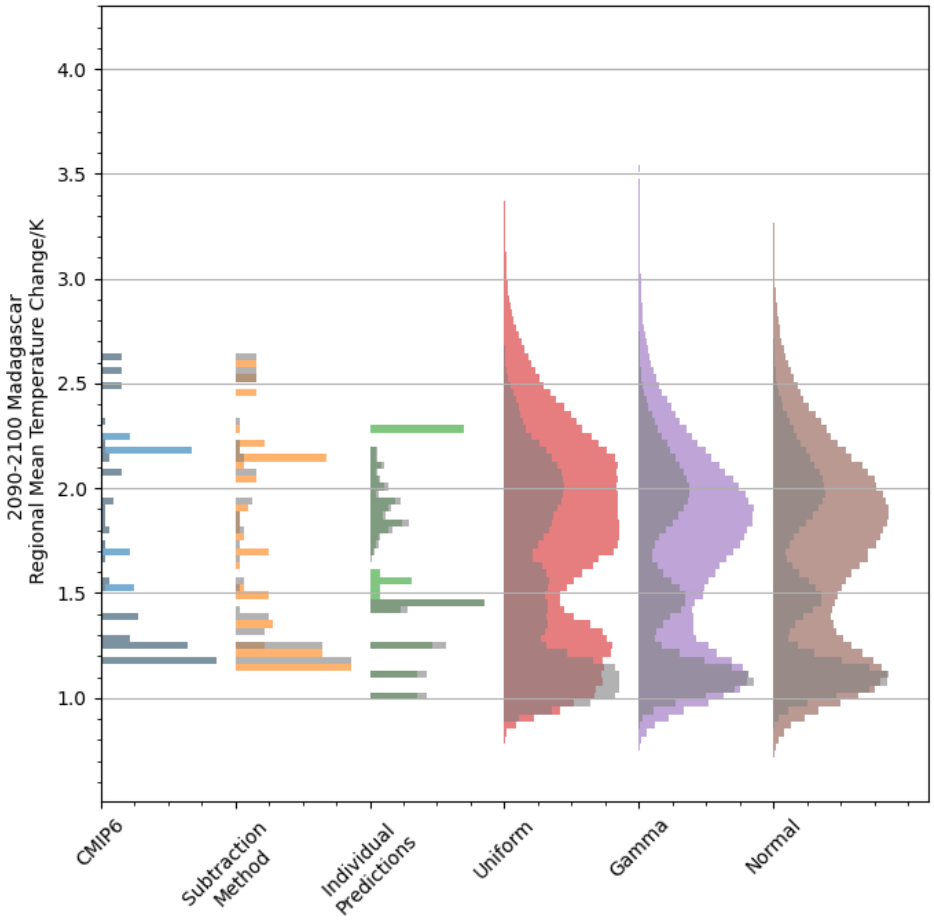


Fig. 36 Histograms of the 2090-2100 regional mean temperature in the CMIP SSP245 runs and the large AMOC decline scenario (-12Sv) for Madagascar as in Figure 3

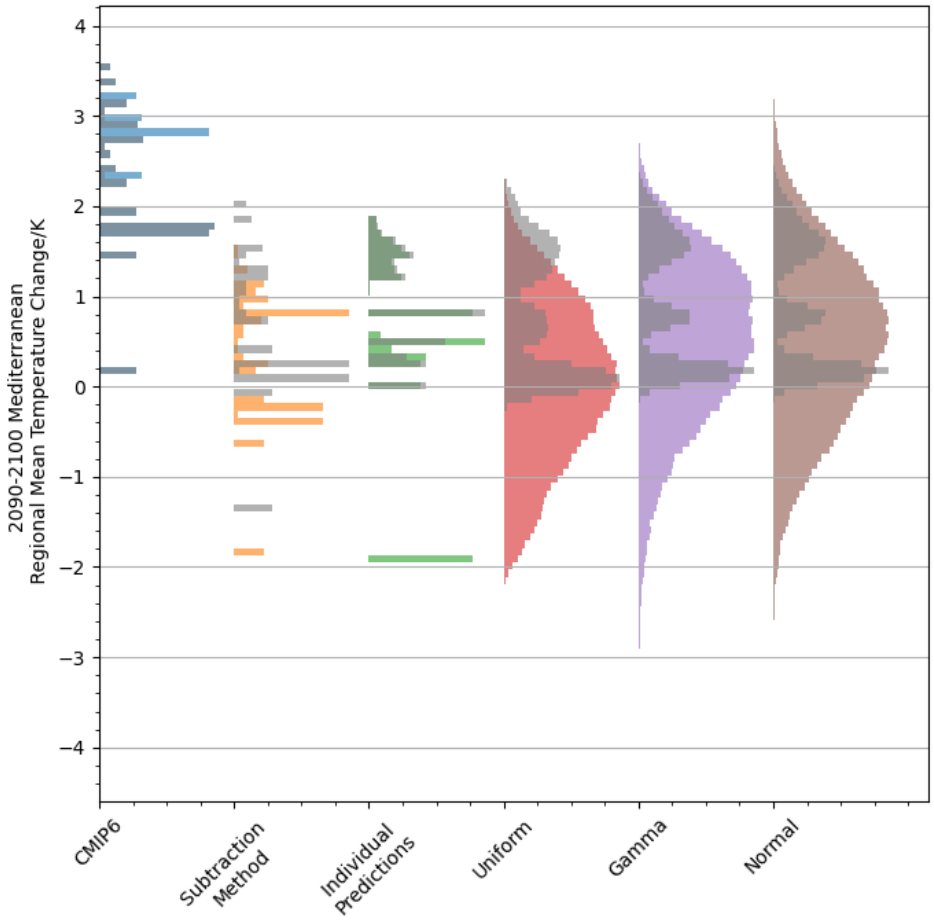


Fig. 37 Histograms of the 2090-2100 regional mean temperature in the CMIP SSP245 runs and the large AMOC decline scenario (-12Sv) for the Mediterranean as in Figure 3

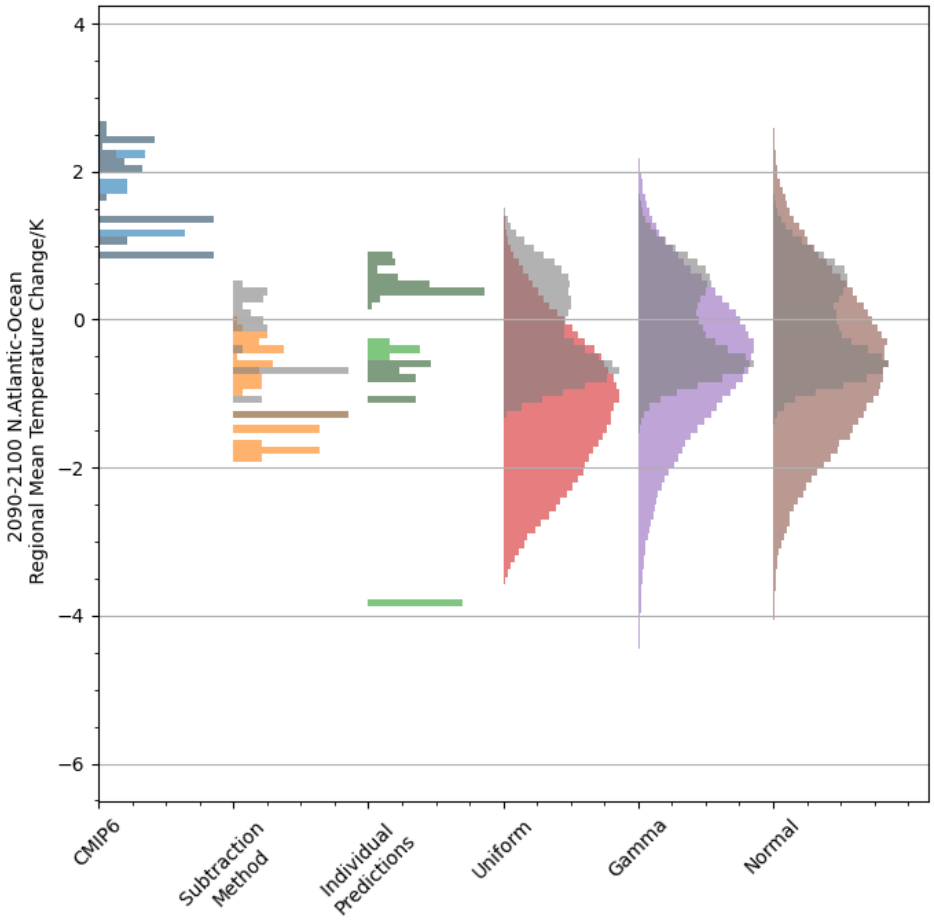


Fig. 38 Histograms of the 2090-2100 regional mean temperature in the CMIP SSP245 runs and the large AMOC decline scenario (-12Sv) for the North Atlantic Ocean as in Figure 3

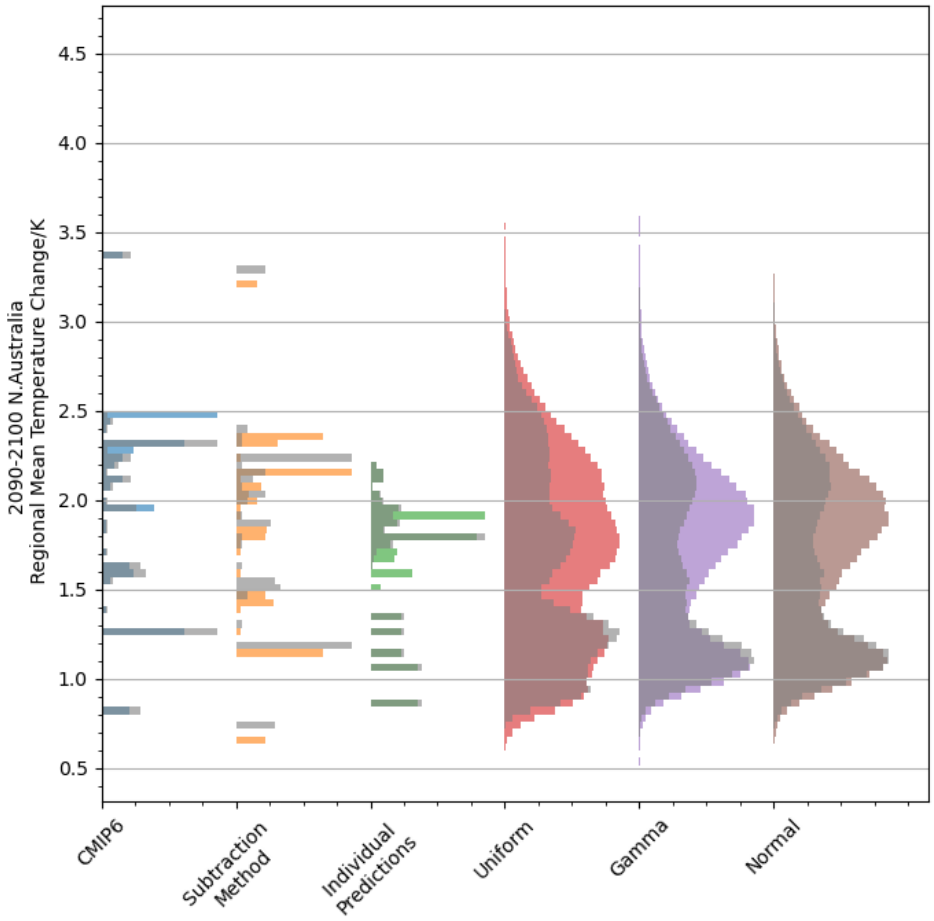


Fig. 39 Histograms of the 2090-2100 regional mean temperature in the CMIP SSP245 runs and the large AMOC decline scenario (-12Sv) for North Australia as in Figure 3

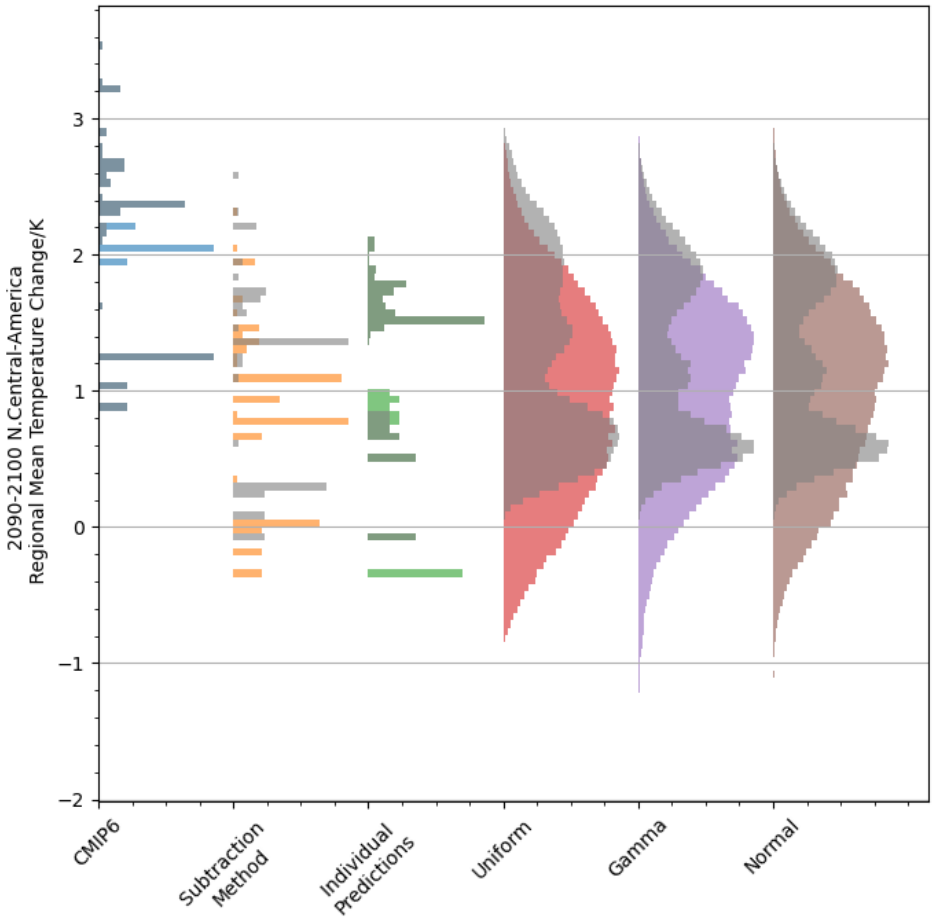


Fig. 40 Histograms of the 2090-2100 regional mean temperature in the CMIP SSP245 runs and the large AMOC decline scenario (-12Sv) for North Central America as in Figure 3

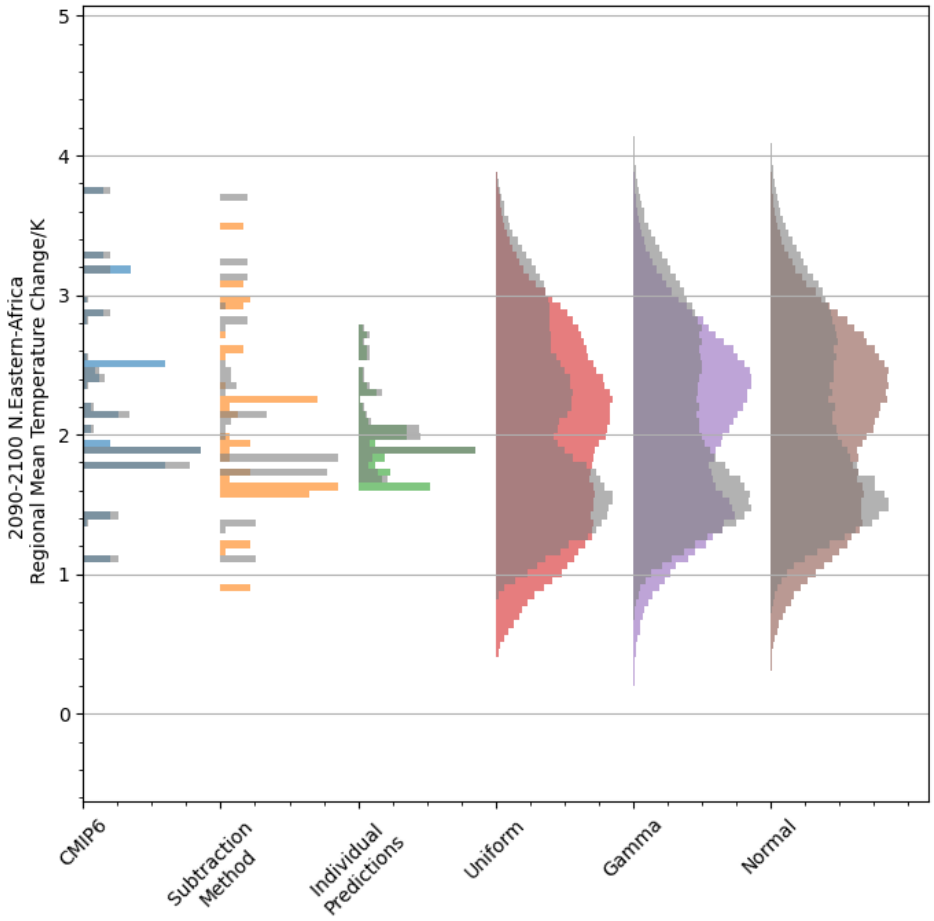


Fig. 41 Histograms of the 2090-2100 regional mean temperature in the CMIP SSP245 runs and the large AMOC decline scenario (-12Sv) for North Eastern Africa as in Figure 3

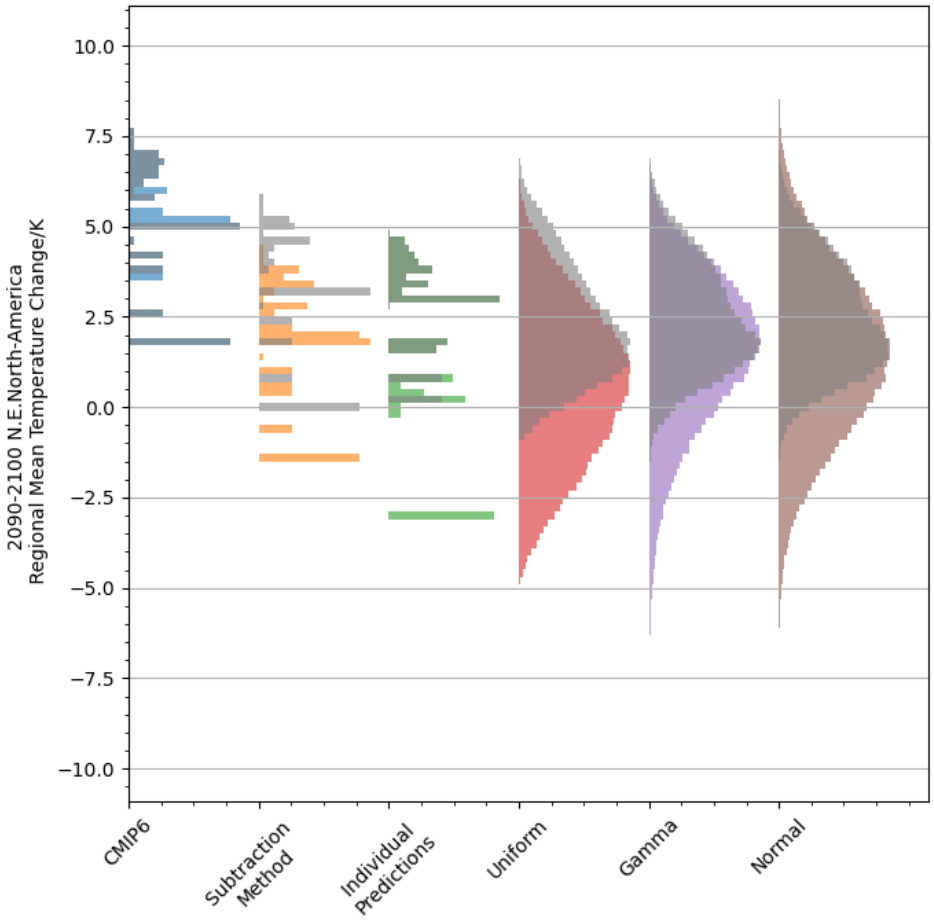


Fig. 42 Histograms of the 2090-2100 regional mean temperature in the CMIP SSP245 runs and the large AMOC decline scenario (-12Sv) for North Eastern North America as in Figure 3

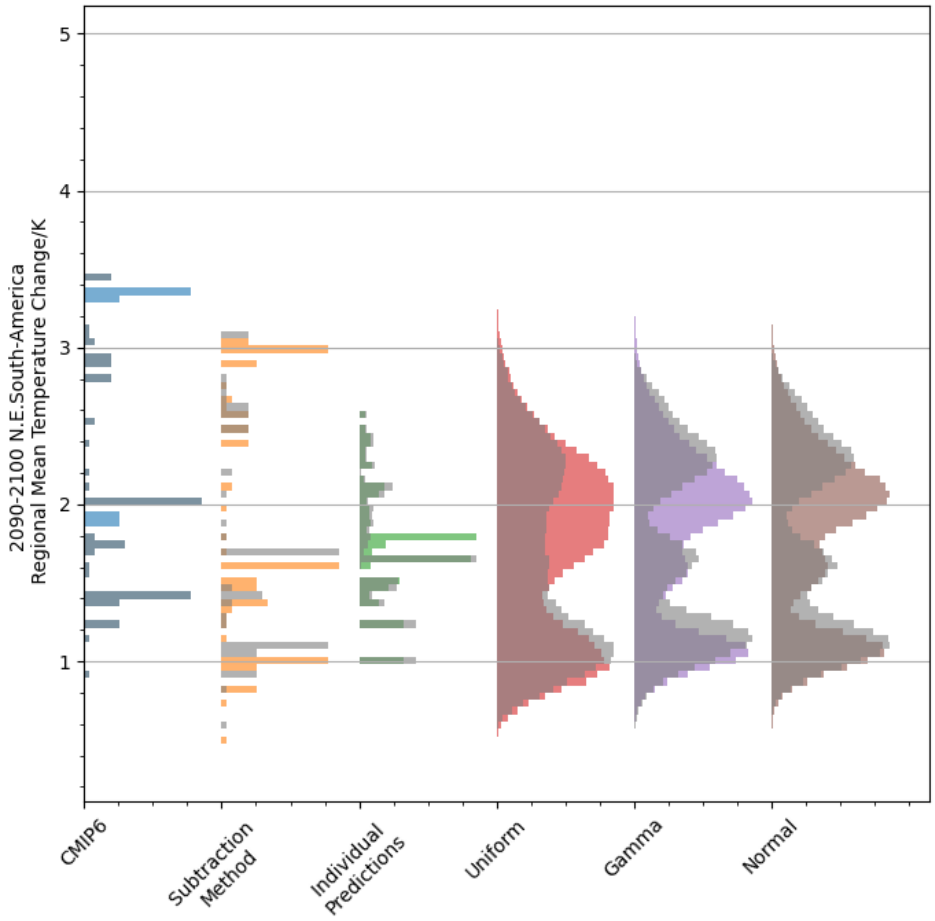


Fig. 43 Histograms of the 2090-2100 regional mean temperature in the CMIP SSP245 runs and the large AMOC decline scenario (-12Sv) for North Eastern South America as in Figure 3

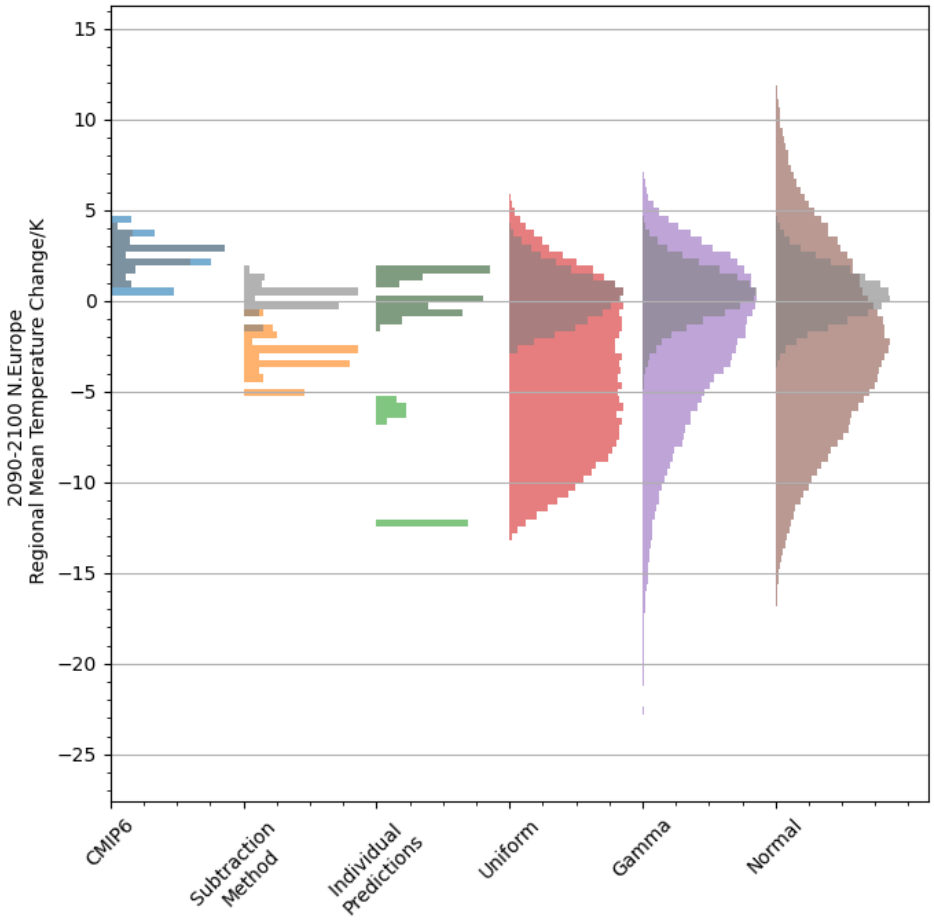


Fig. 44 Histograms of the 2090-2100 regional mean temperature in the CMIP SSP245 runs and the large AMOC decline scenario (-12Sv) for Northern Europe as in Figure 3

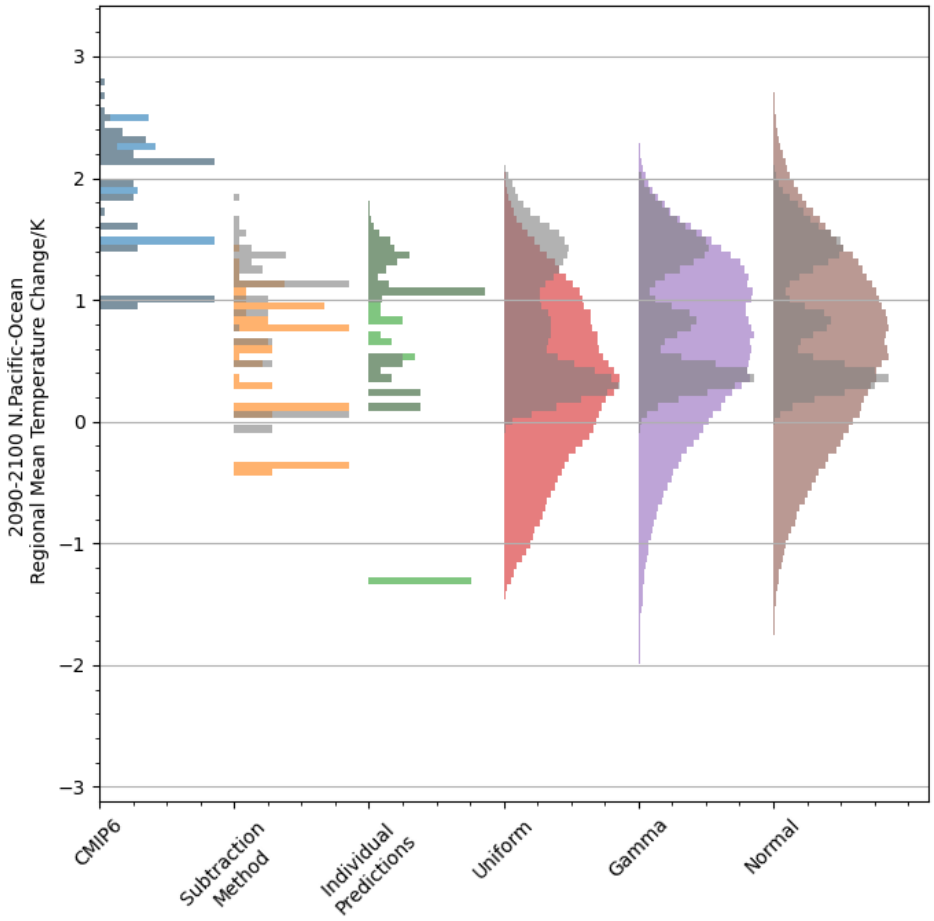


Fig. 45 Histograms of the 2090-2100 regional mean temperature in the CMIP SSP245 runs and the large AMOC decline scenario (-12Sv) for the North Pacific Ocean as in Figure 3

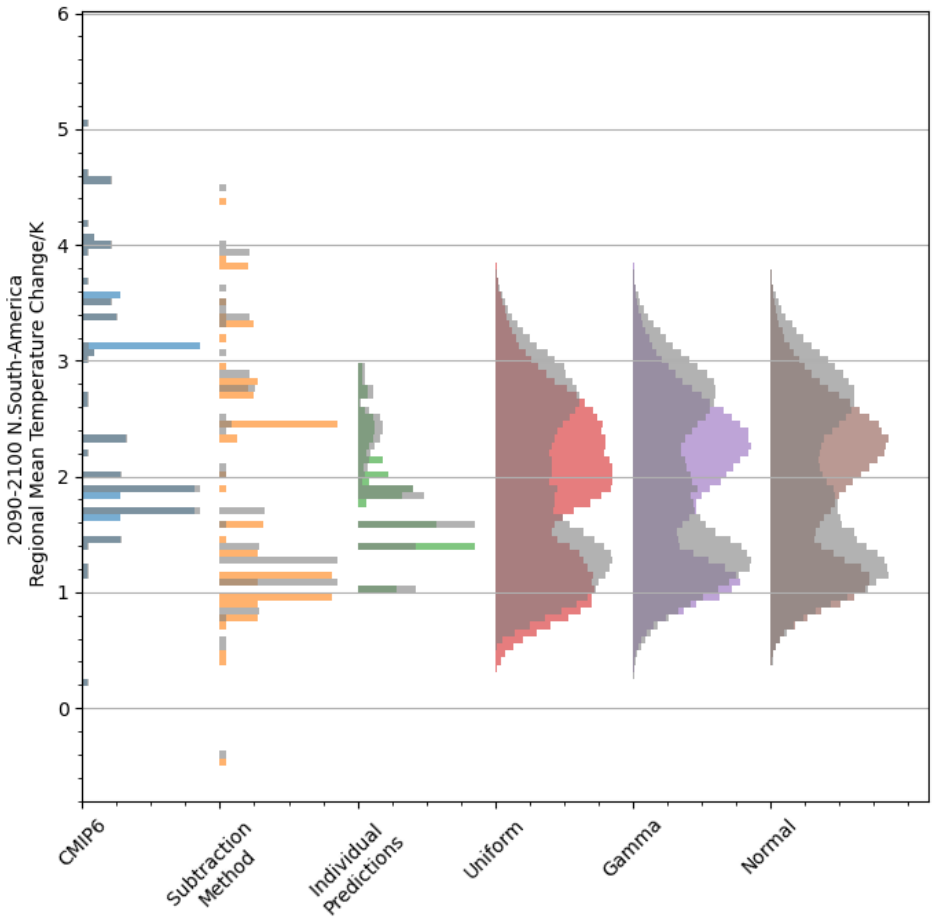


Fig. 46 Histograms of the 2090-2100 regional mean temperature in the CMIP SSP245 runs and the large AMOC decline scenario (-12Sv) for Northern South America as in Figure 3

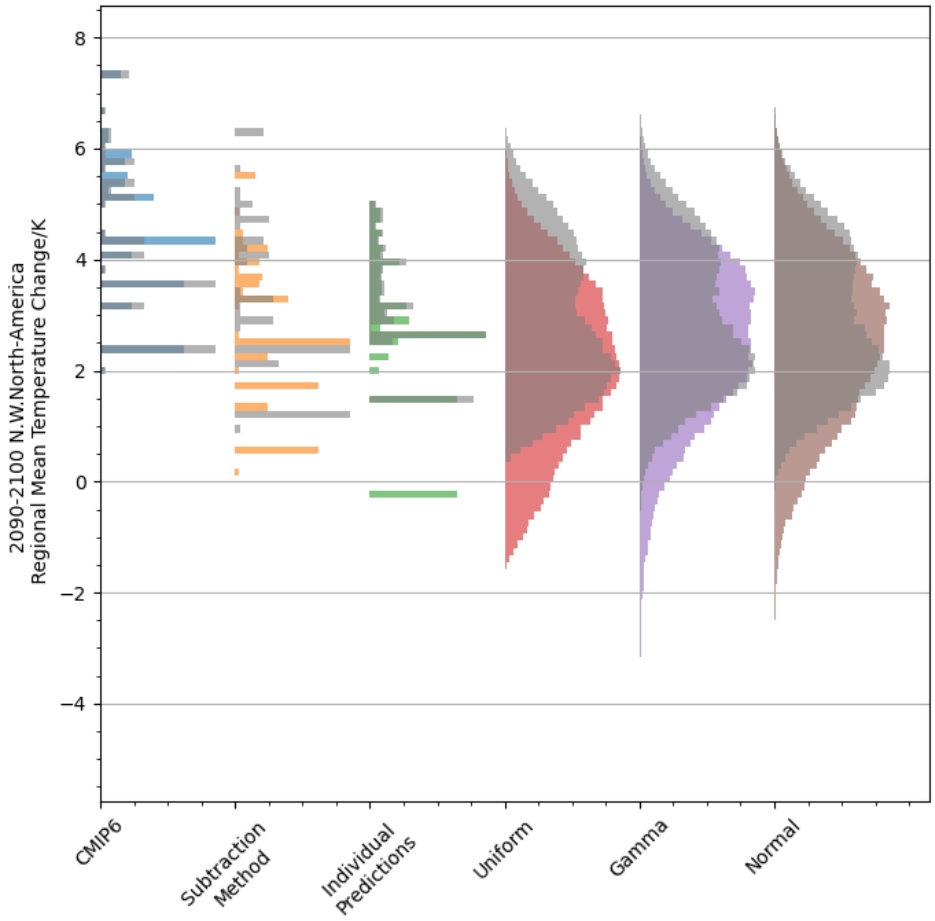


Fig. 47 Histograms of the 2090-2100 regional mean temperature in the CMIP SSP245 runs and the large AMOC decline scenario (-12Sv) for North Western North America as in Figure 3

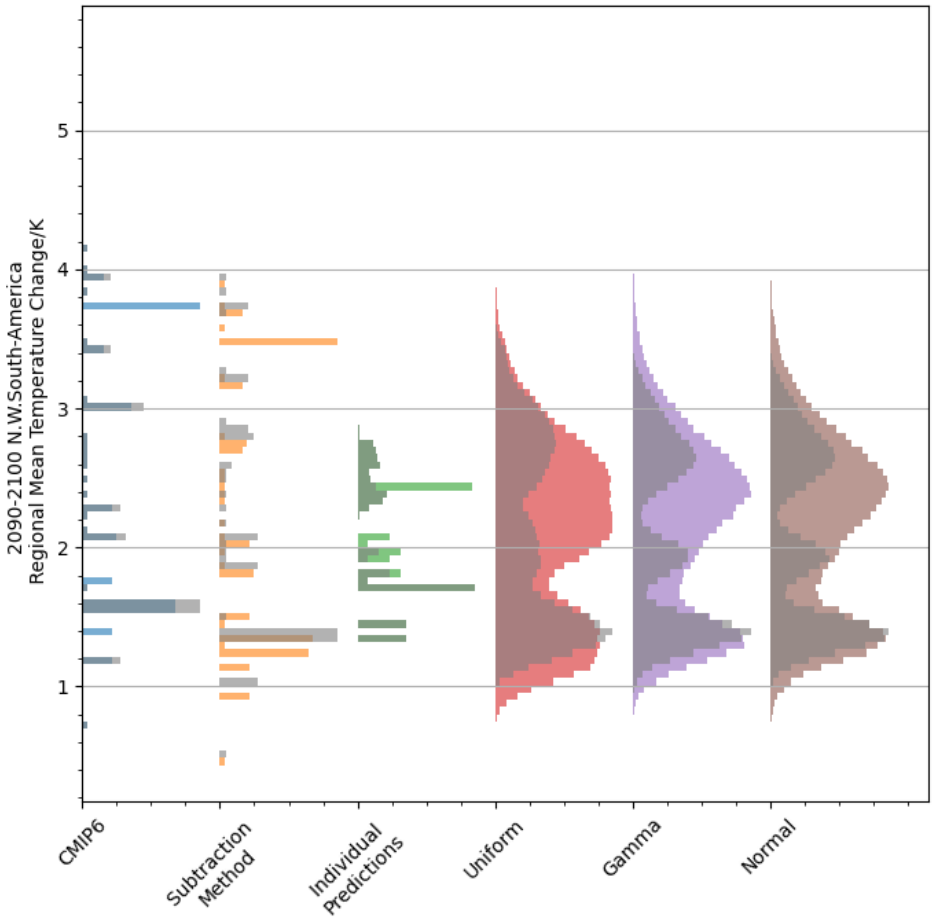


Fig. 48 Histograms of the 2090-2100 regional mean temperature in the CMIP SSP245 runs and the large AMOC decline scenario (-12Sv) for North Western South America as in Figure 3

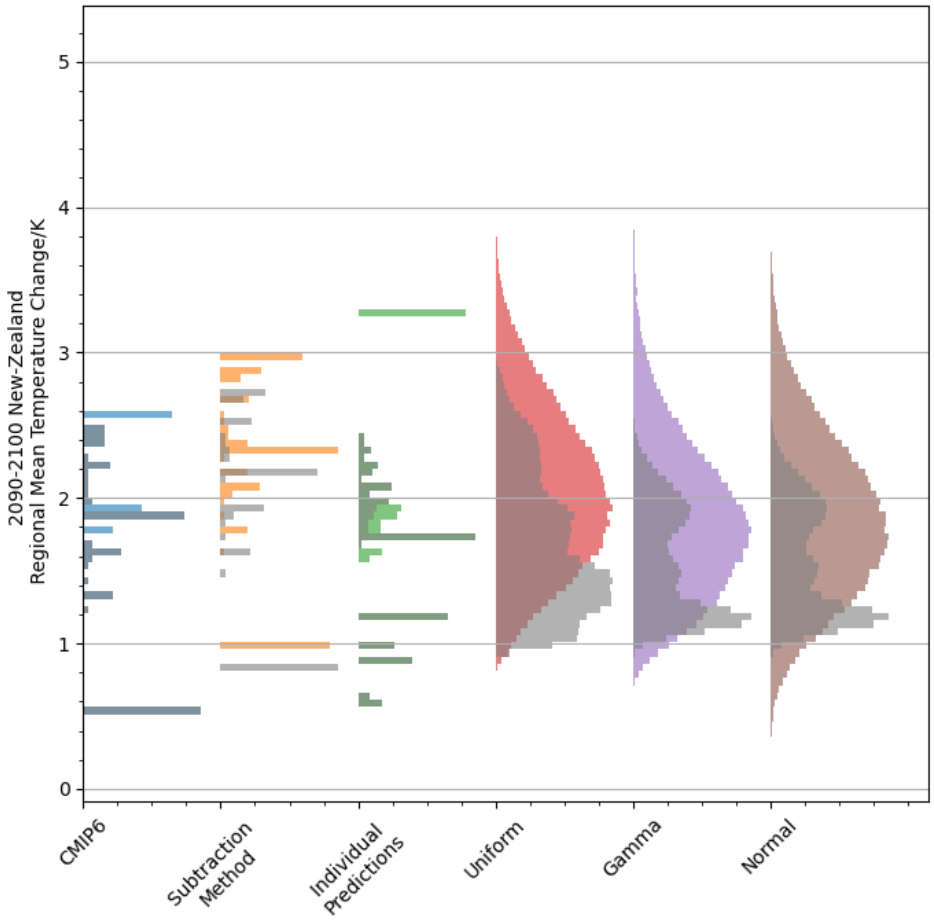


Fig. 49 Histograms of the 2090-2100 regional mean temperature in the CMIP SSP245 runs and the large AMOC decline scenario (-12Sv) for New Zealand as in Figure 3

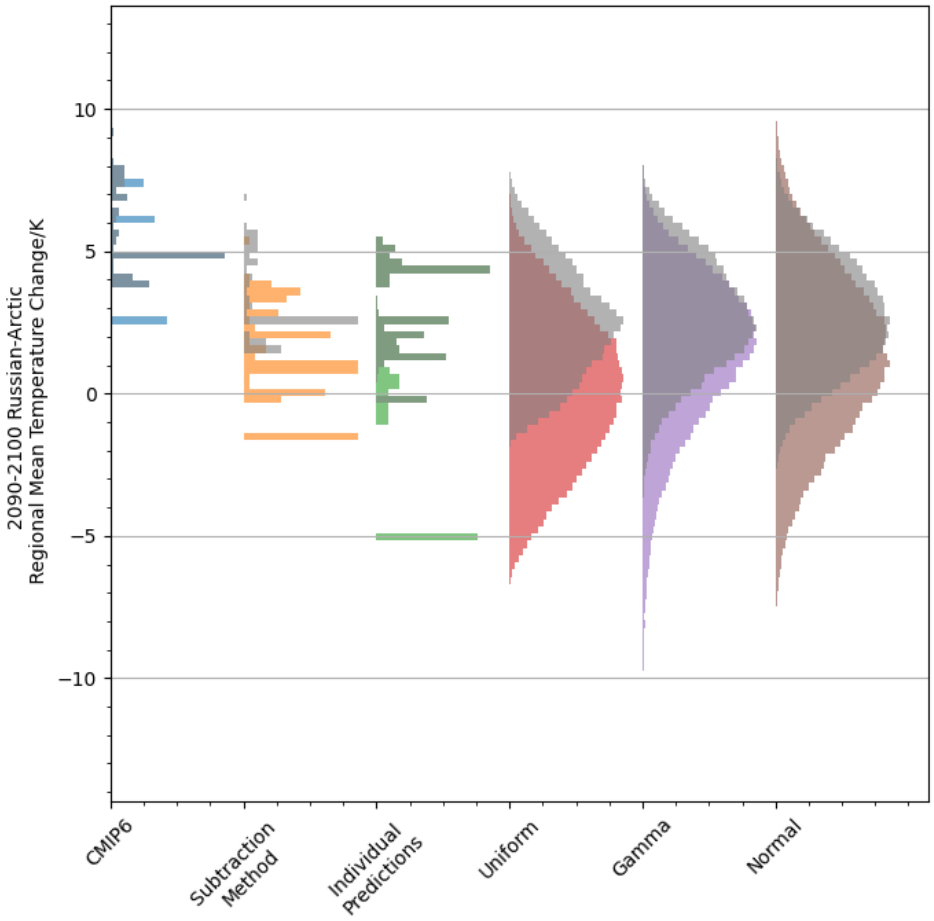


Fig. 50 Histograms of the 2090-2100 regional mean temperature in the CMIP SSP245 runs and the large AMOC decline scenario (-12Sv) for the Russian Arctic Region as in Figure 3

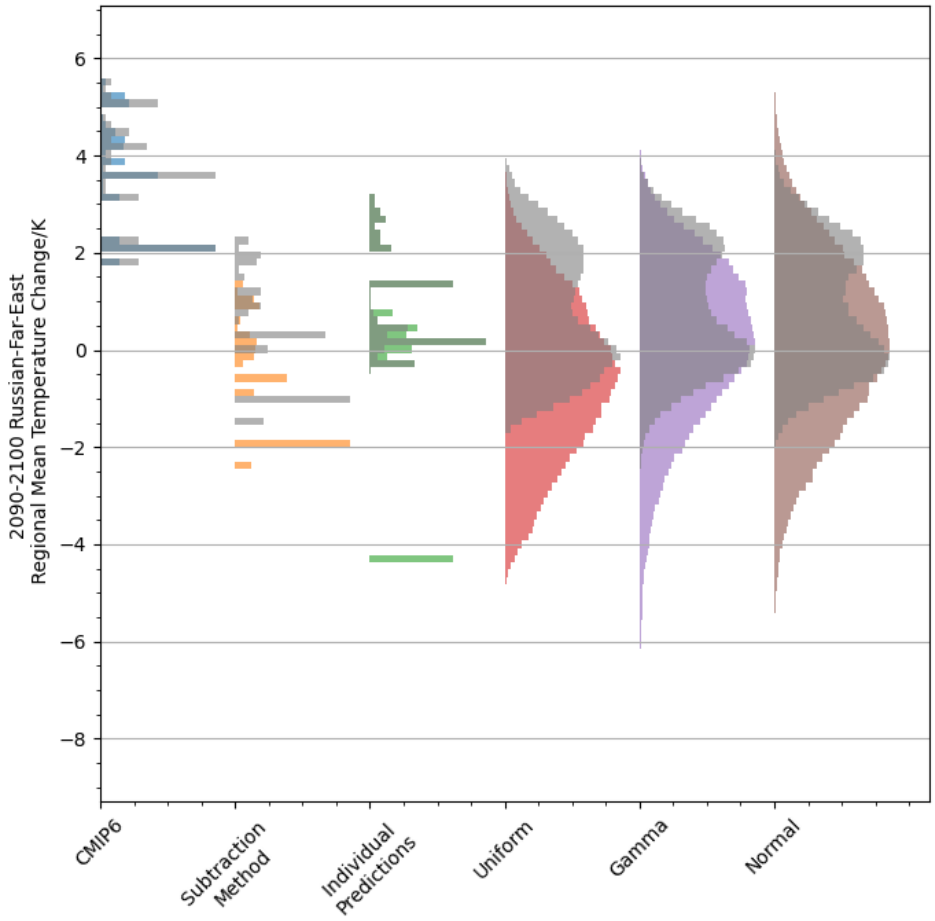


Fig. 51 Histograms of the 2090-2100 regional mean temperature in the CMIP SSP245 runs and the large AMOC decline scenario (-12Sv) for the Russian Far East as in Figure 3

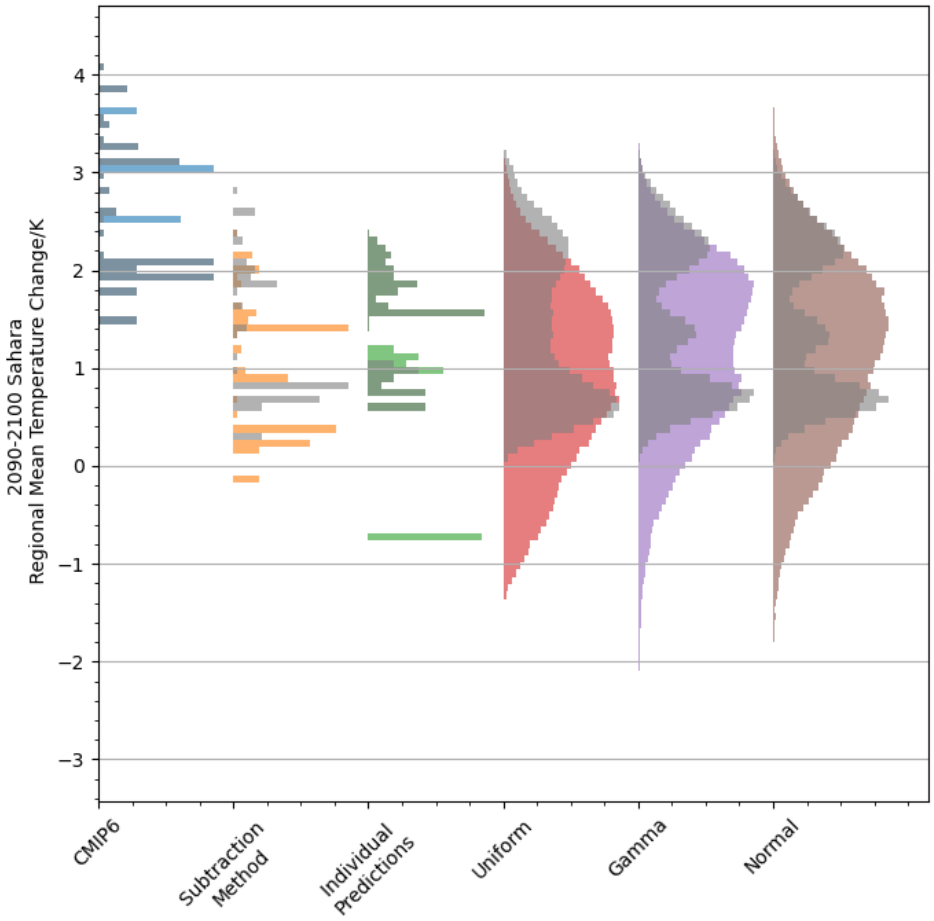


Fig. 52 Histograms of the 2090-2100 regional mean temperature in the CMIP SSP245 runs and the large AMOC decline scenario (-12Sv) for the Sahara as in Figure 3

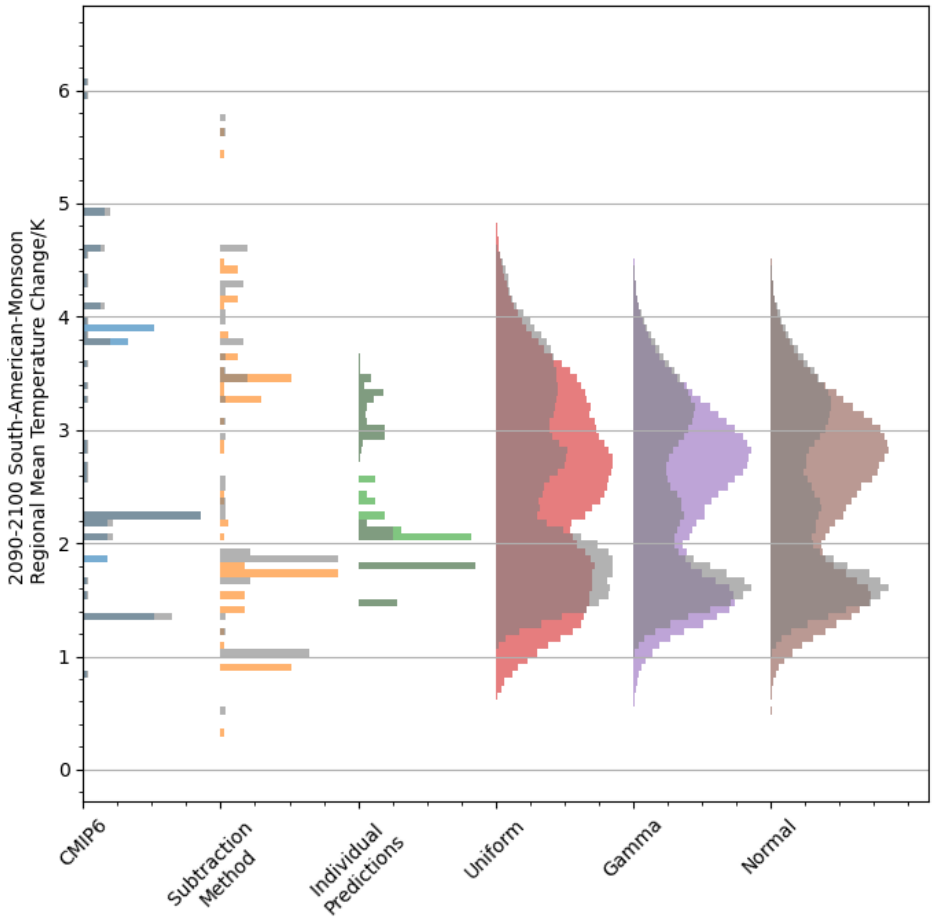


Fig. 53 Histograms of the 2090-2100 regional mean temperature in the CMIP SSP245 runs and the large AMOC decline scenario (-12Sv) for the South American Monsoon Region as in Figure 3

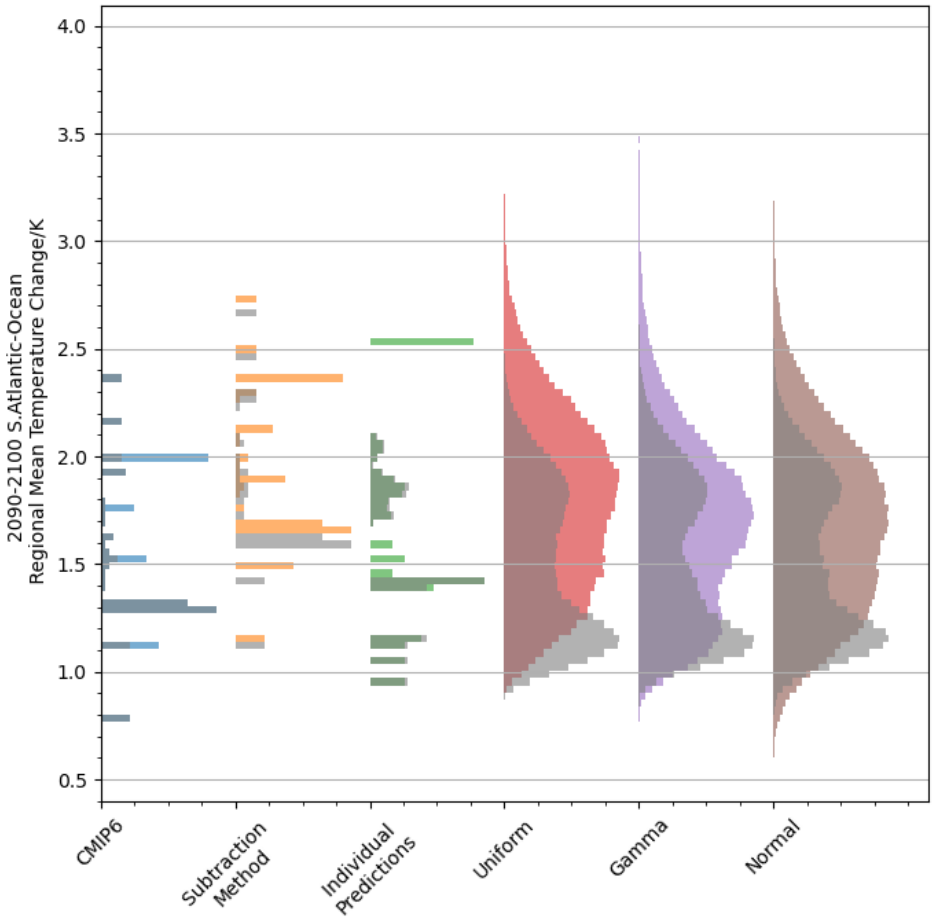


Fig. 54 Histograms of the 2090-2100 regional mean temperature in the CMIP SSP245 runs and the large AMOC decline scenario (-12Sv) for South Atlantic Ocean as in Figure 3

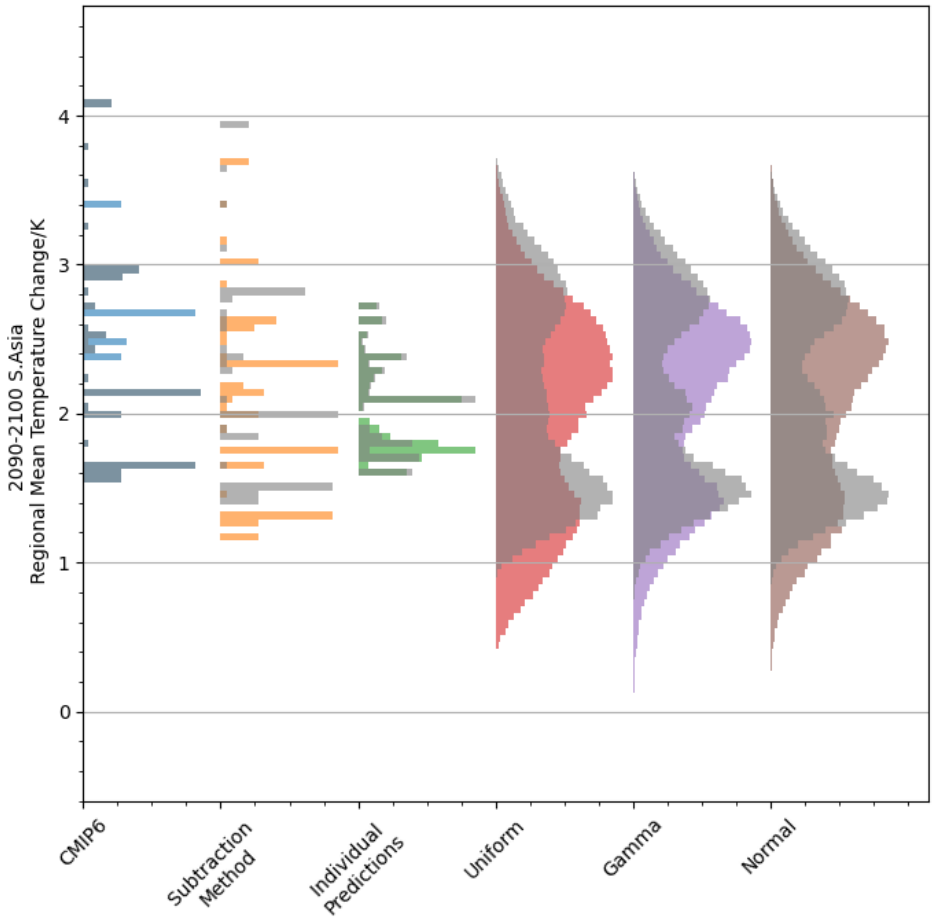


Fig. 55 Histograms of the 2090-2100 regional mean temperature in the CMIP SSP245 runs and the large AMOC decline scenario (-12Sv) for South Asia as in Figure 3

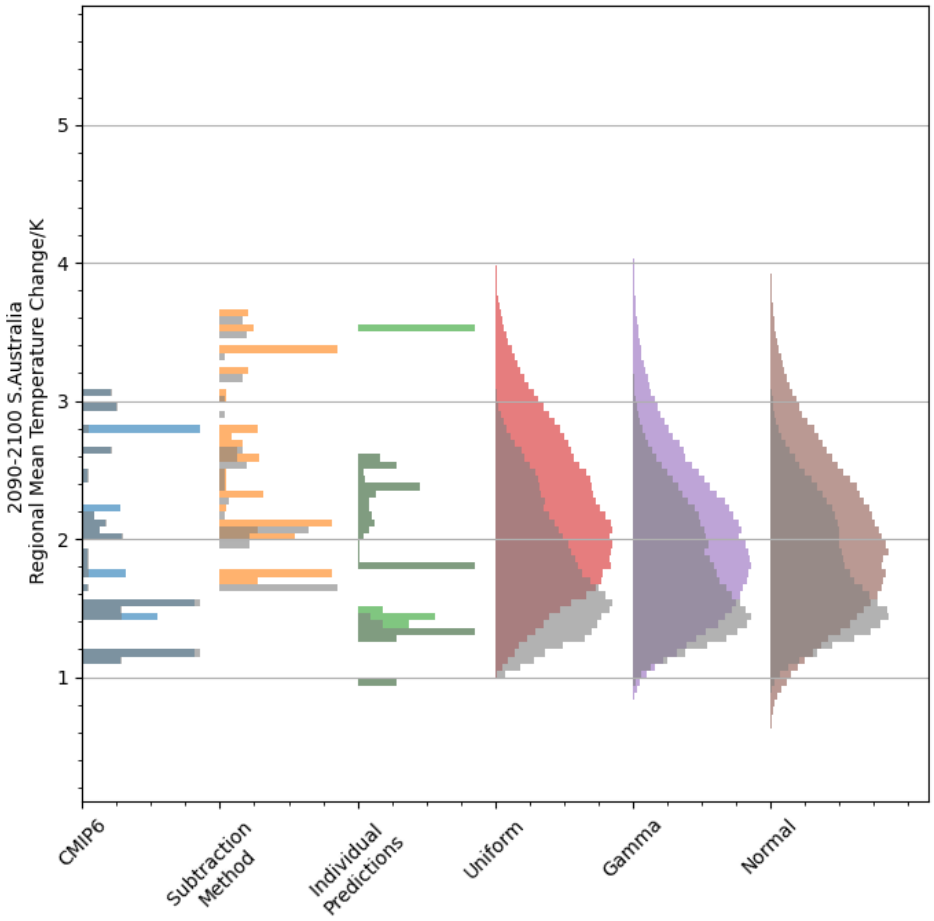


Fig. 56 Histograms of the 2090-2100 regional mean temperature in the CMIP SSP245 runs and the large AMOC decline scenario (-12Sv) for South Australia as in Figure 3

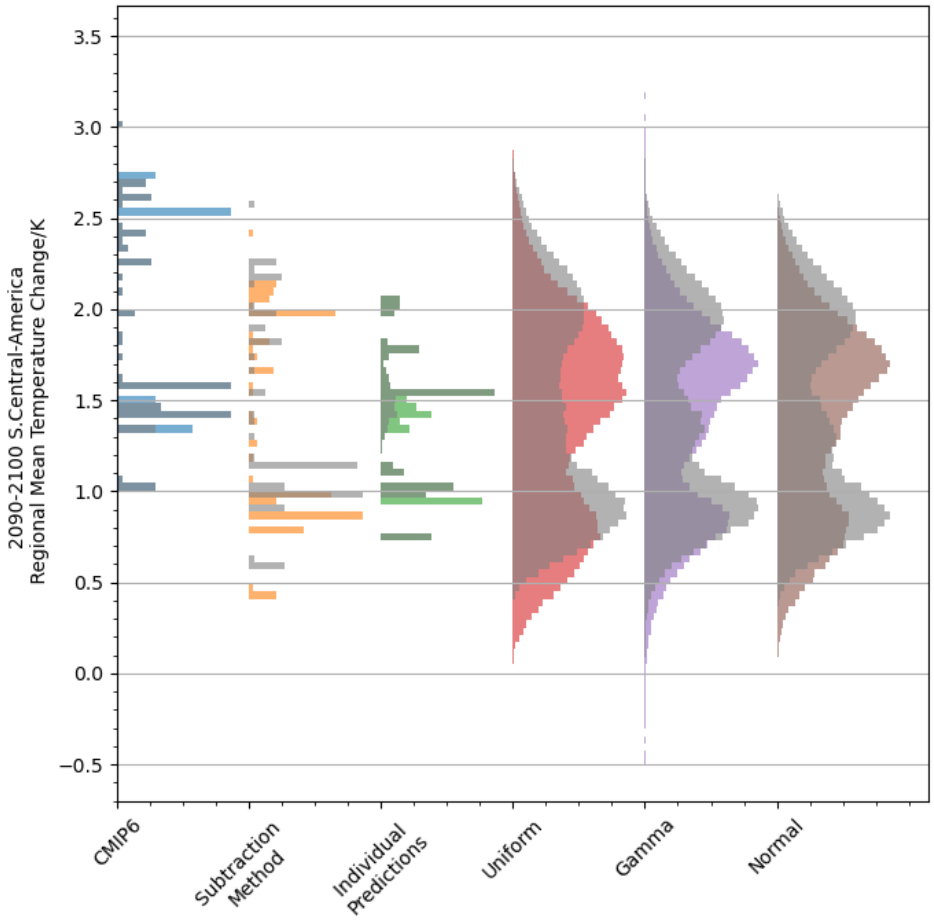


Fig. 57 Histograms of the 2090-2100 regional mean temperature in the CMIP SSP245 runs and the large AMOC decline scenario (-12Sv) for Southern Central America as in Figure 3

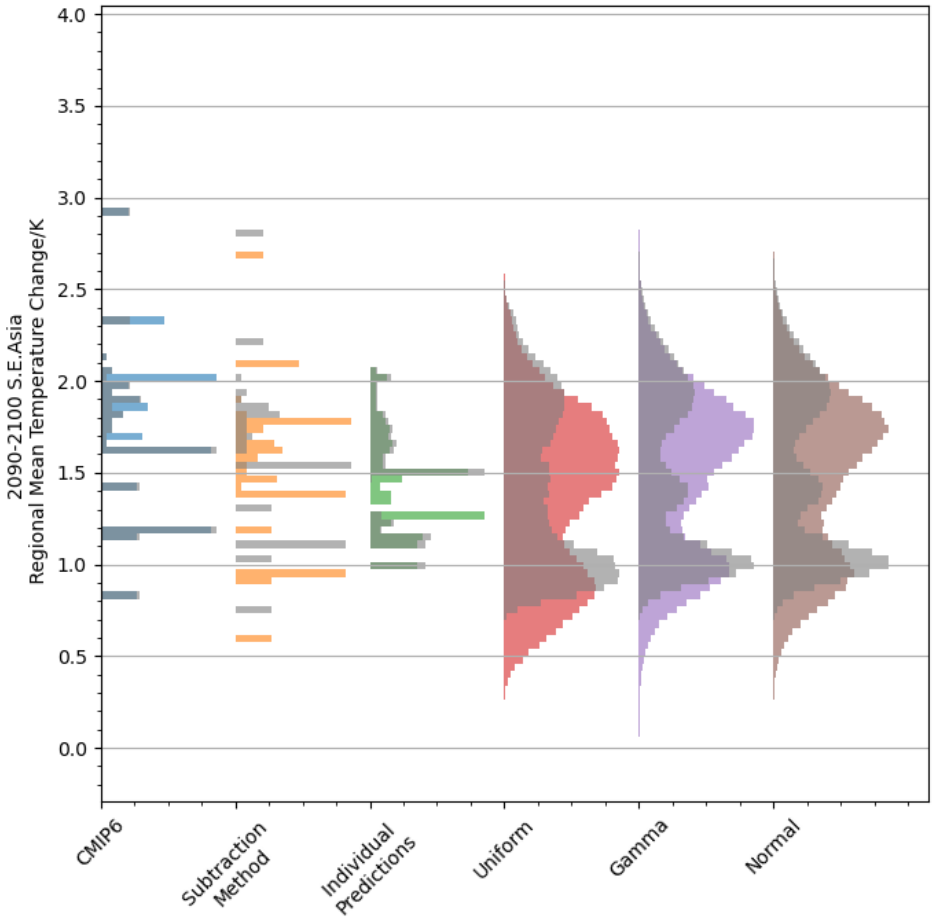


Fig. 58 Histograms of the 2090-2100 regional mean temperature in the CMIP SSP245 runs and the large AMOC decline scenario (-12Sv) for South East Asia as in Figure 3

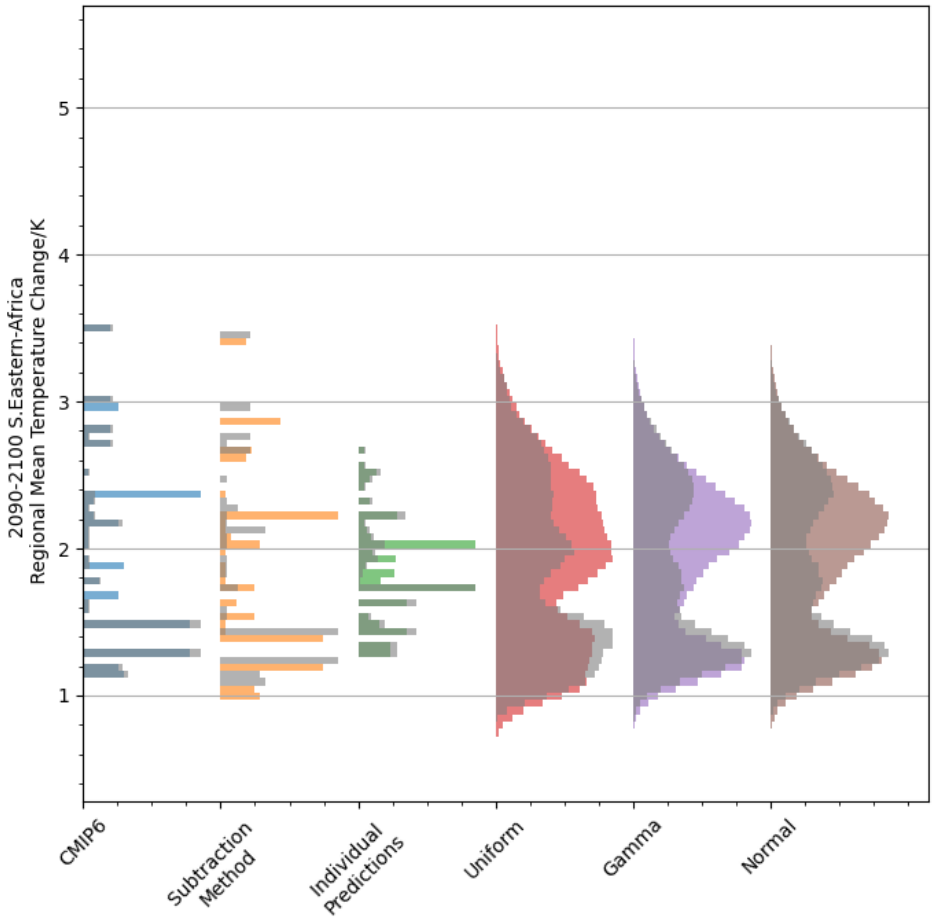


Fig. 59 Histograms of the 2090-2100 regional mean temperature in the CMIP SSP245 runs and the large AMOC decline scenario (-12Sv) for South Eastern Africa as in Figure 3

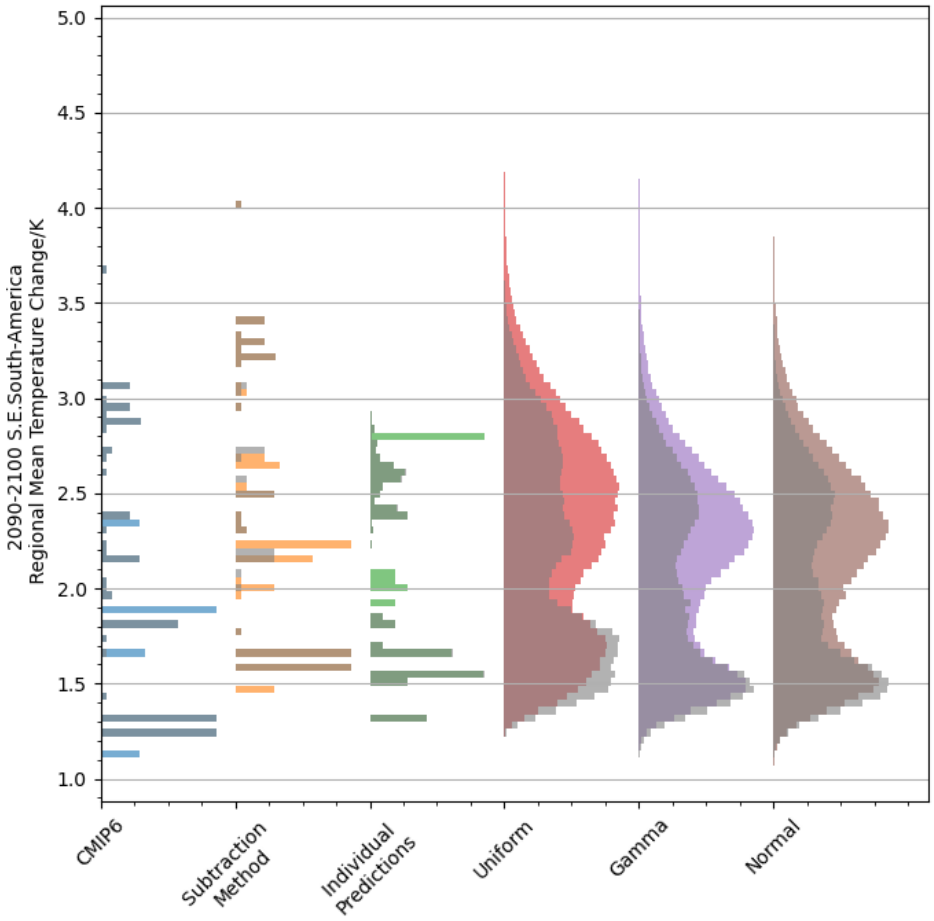


Fig. 60 Histograms of the 2090-2100 regional mean temperature in the CMIP SSP245 runs and the large AMOC decline scenario (-12Sv) for South Eastern South America as in Figure 3

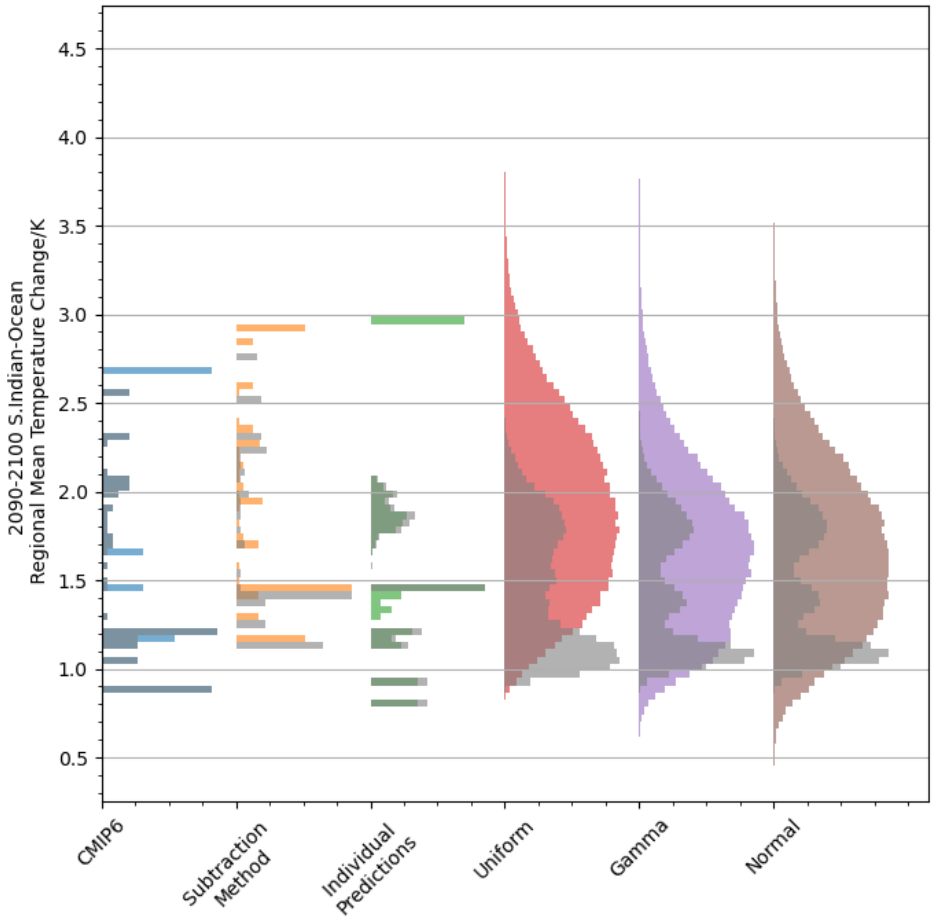


Fig. 61 Histograms of the 2090-2100 regional mean temperature in the CMIP SSP245 runs and the large AMOC decline scenario (-12Sv) for the South Indian Ocean as in Figure 3

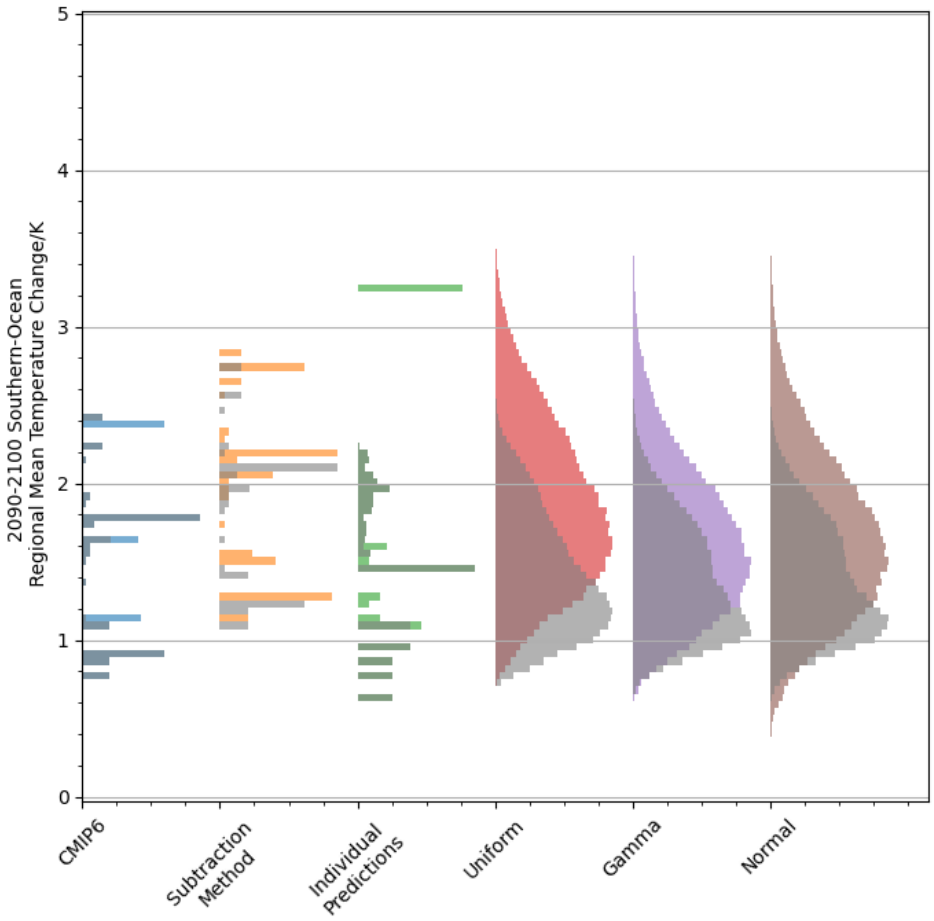


Fig. 62 Histograms of the 2090-2100 regional mean temperature in the CMIP SSP245 runs and the large AMOC decline scenario (-12Sv) for the Southern Ocean as in Figure 3

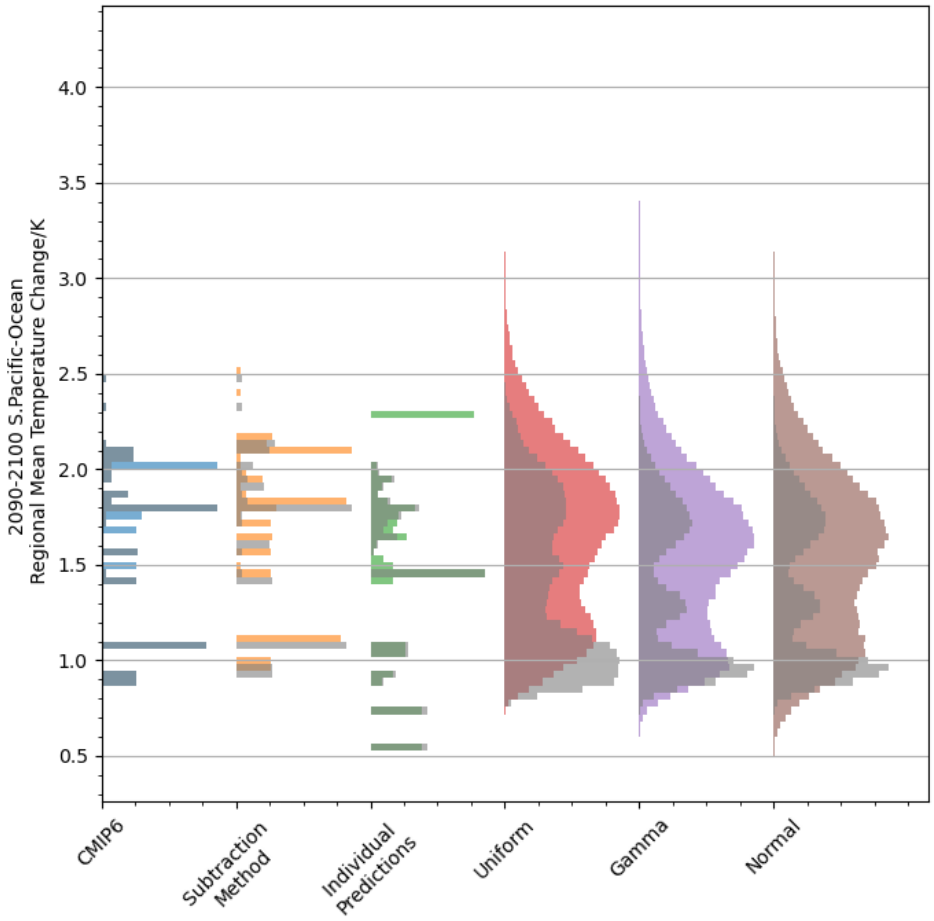


Fig. 63 Histograms of the 2090-2100 regional mean temperature in the CMIP SSP245 runs and the large AMOC decline scenario (-12Sv) for the South Pacific Ocean as in Figure 3

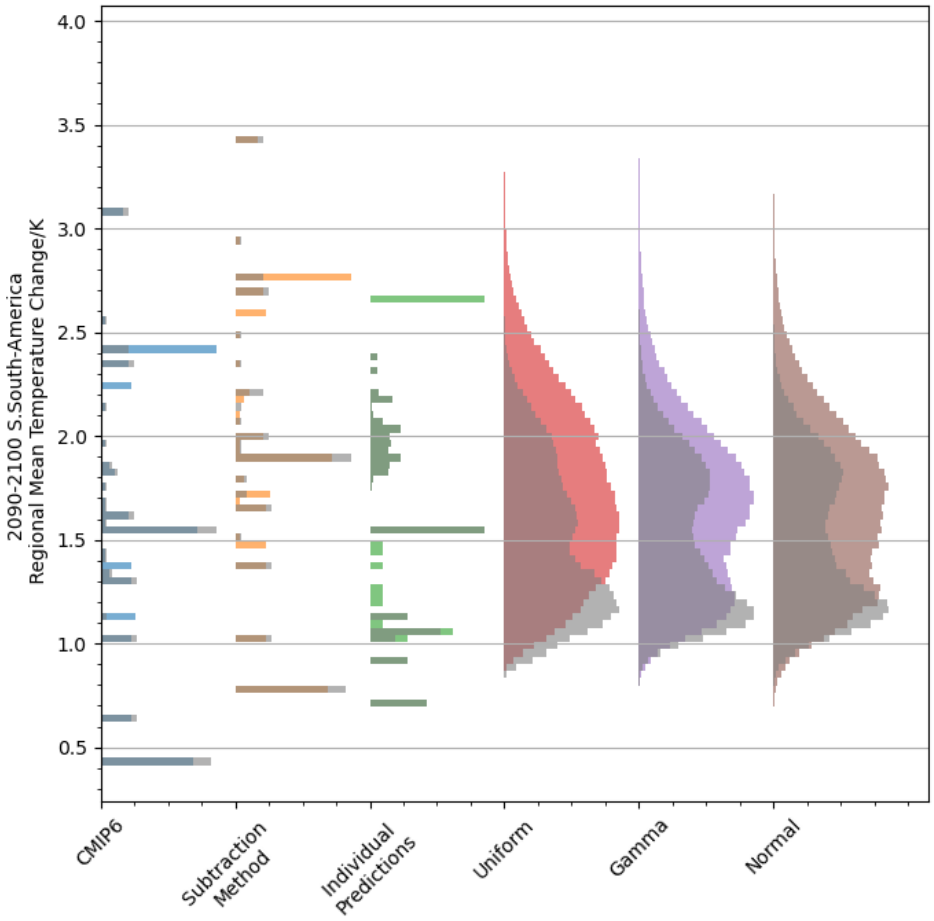


Fig. 64 Histograms of the 2090-2100 regional mean temperature in the CMIP SSP245 runs and the large AMOC decline scenario (-12Sv) for Southern South America as in Figure 3

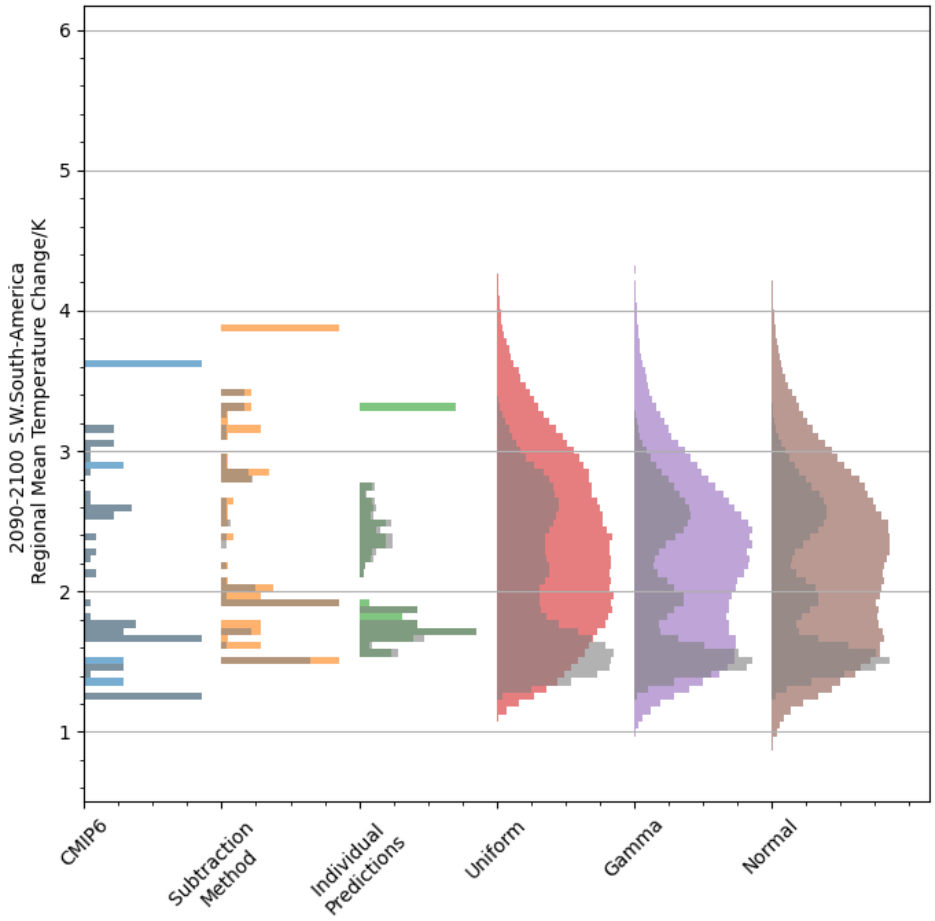


Fig. 65 Histograms of the 2090-2100 regional mean temperature in the CMIP SSP245 runs and the large AMOC decline scenario (-12Sv) for South Western South America as in Figure 3

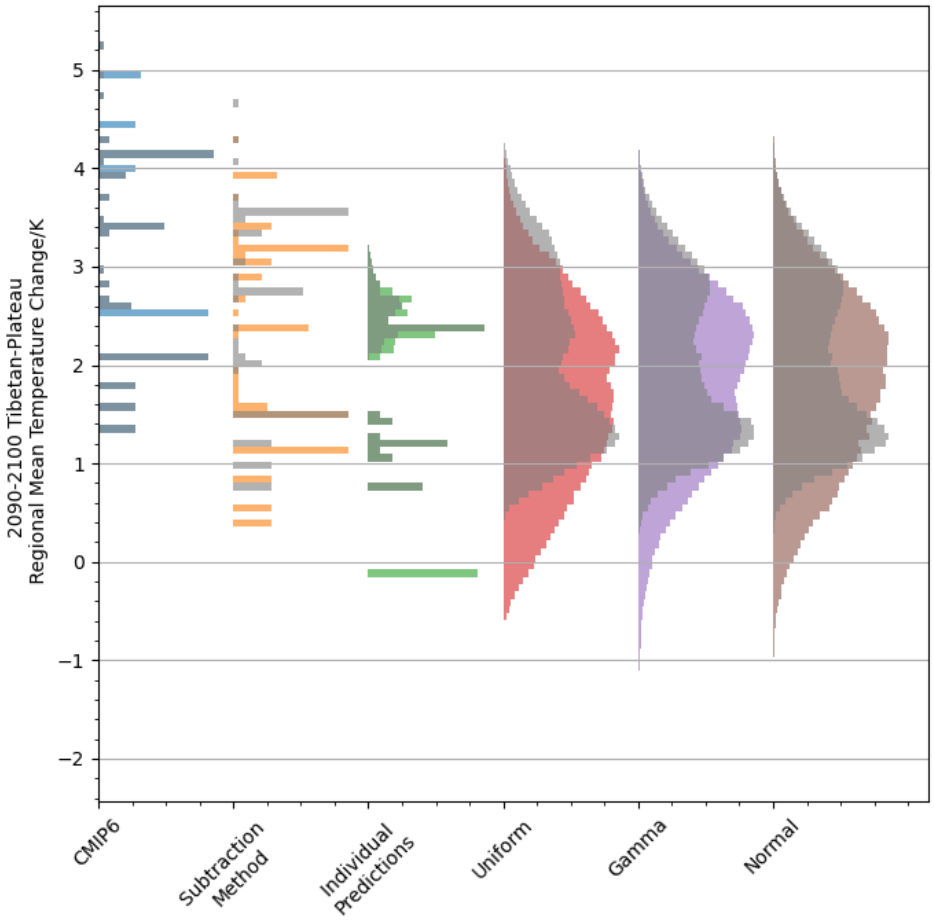


Fig. 66 Histograms of the 2090-2100 regional mean temperature in the CMIP SSP245 runs and the large AMOC decline scenario (-12Sv) for the Tibetan Plateau as in Figure 3

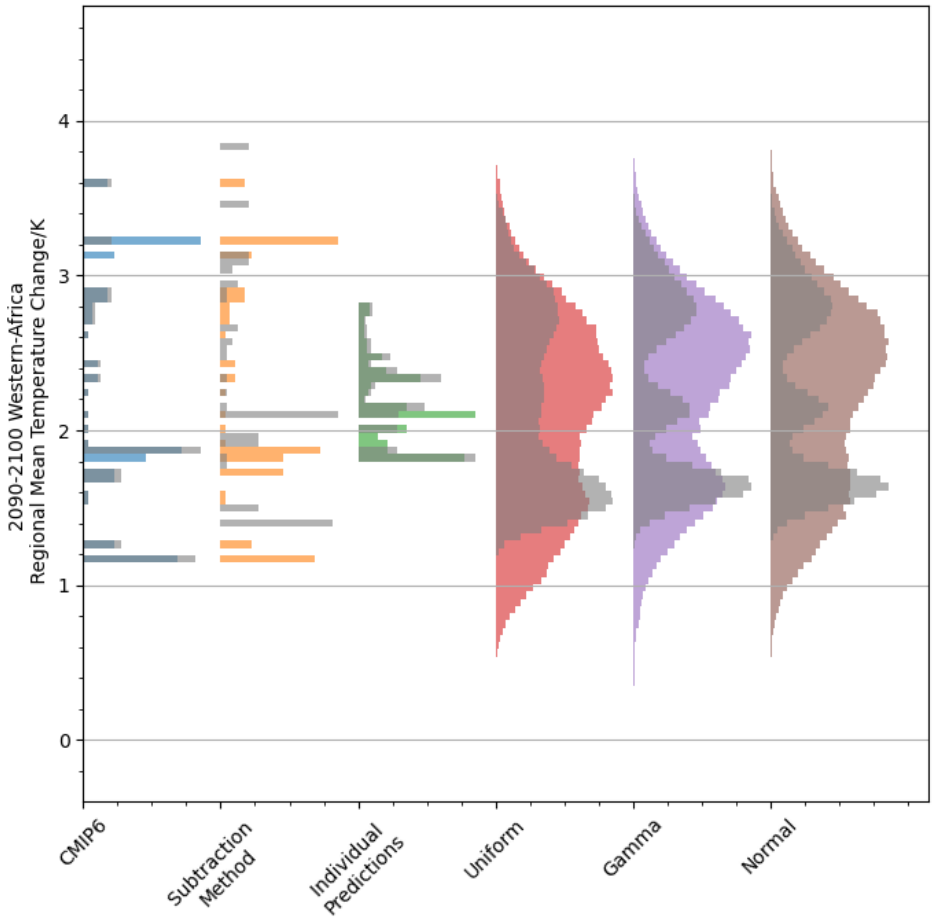


Fig. 67 Histograms of the 2090-2100 regional mean temperature in the CMIP SSP245 runs and the large AMOC decline scenario (-12Sv) for Western Africa as in Figure 3

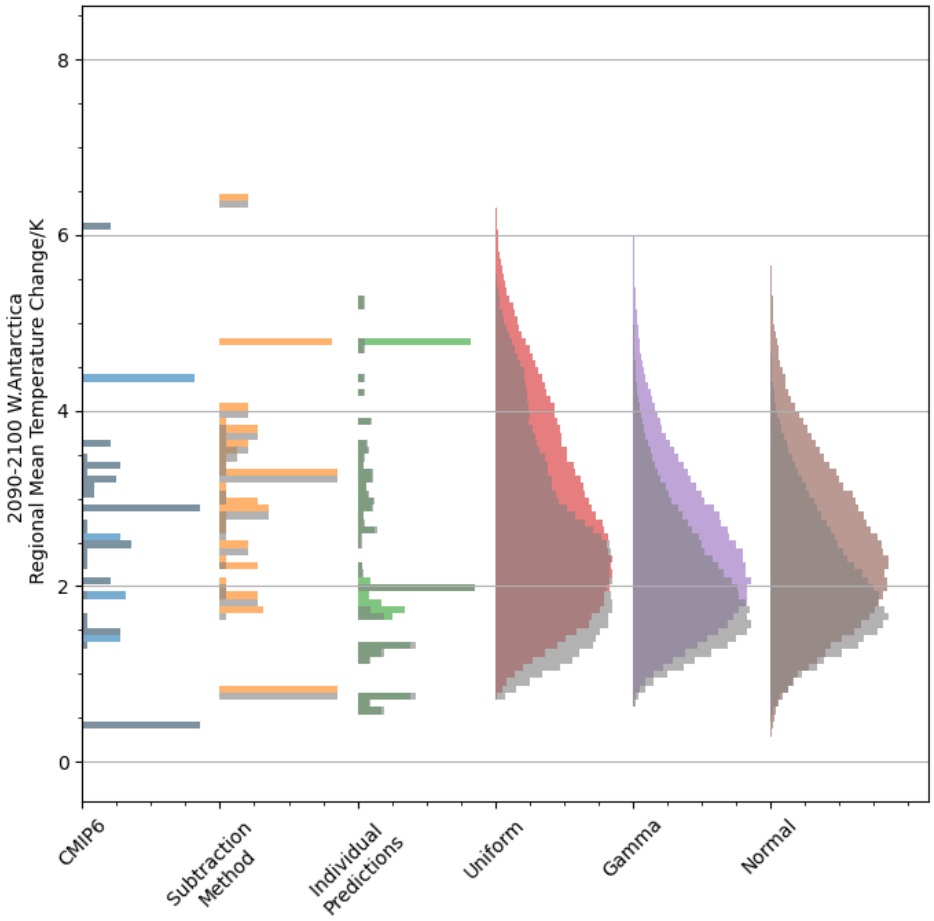


Fig. 68 Histograms of the 2090-2100 regional mean temperature in the CMIP SSP245 runs and the large AMOC decline scenario (-12Sv) for West Antarctica as in Figure 3

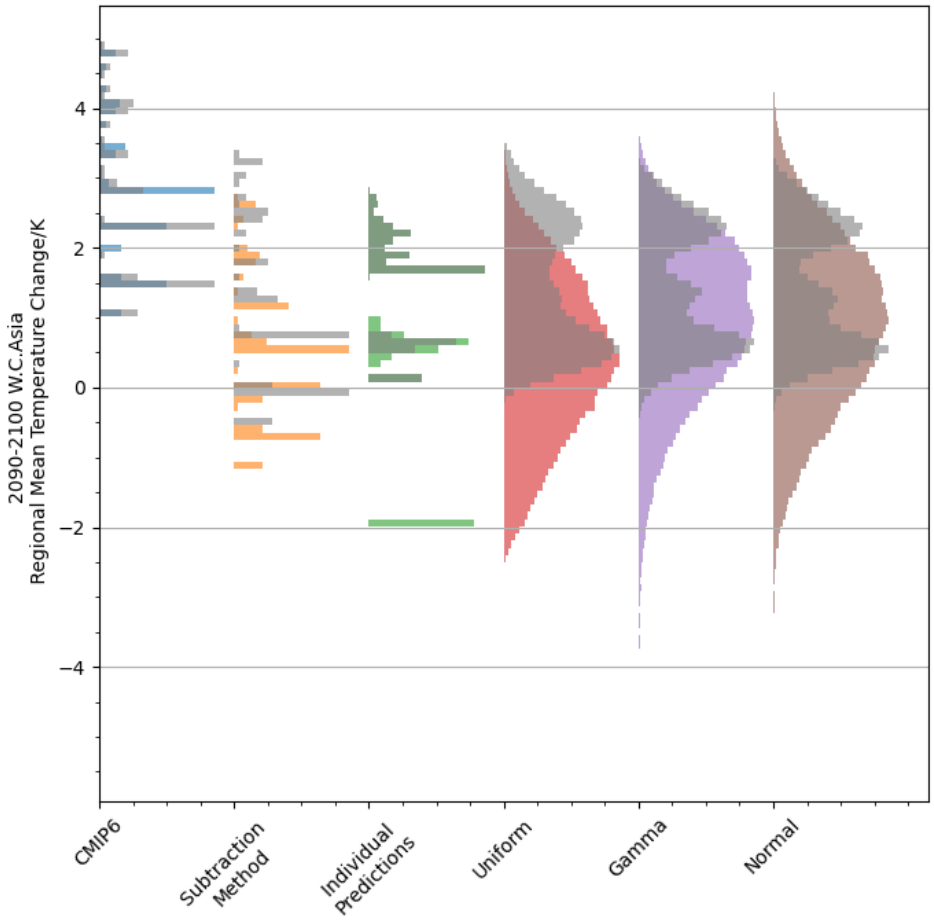


Fig. 69 Histograms of the 2090-2100 regional mean temperature in the CMIP SSP245 runs and the large AMOC decline scenario (-12Sv) for West Central Asia as in Figure 3

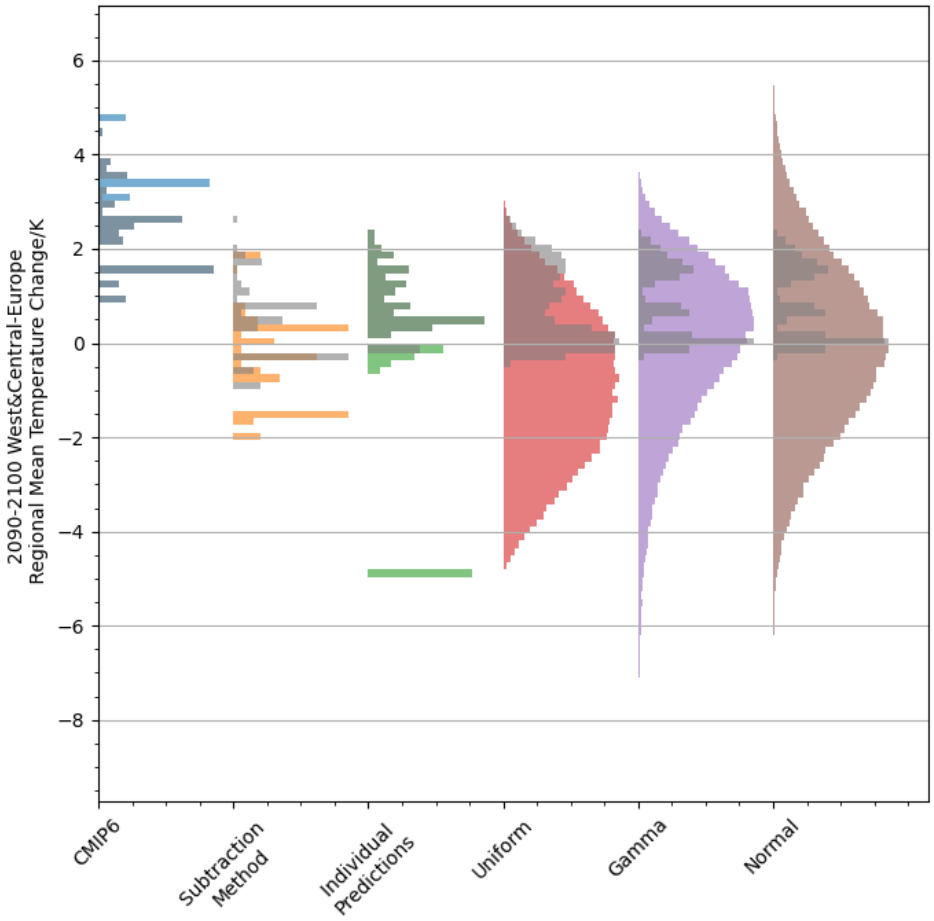


Fig. 70 Histograms of the 2090-2100 regional mean temperature in the CMIP SSP245 runs and the large AMOC decline scenario (-12Sv) for West and Central Europe as in Figure 3

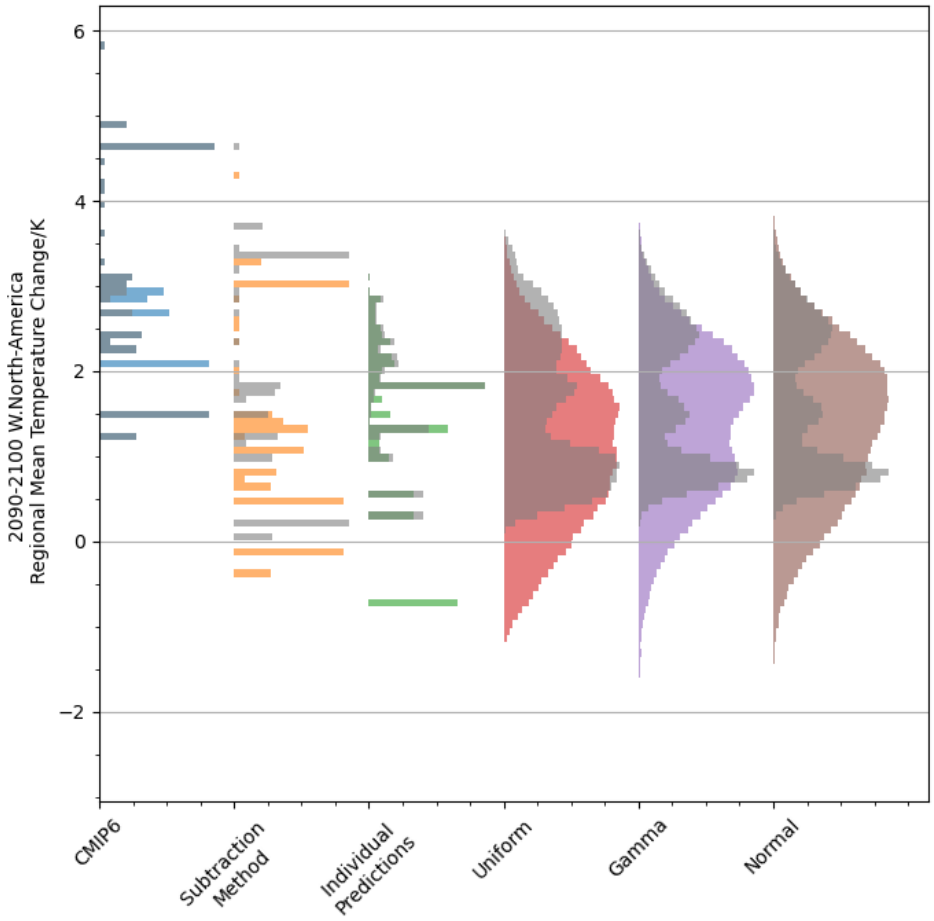


Fig. 71 Histograms of the 2090-2100 regional mean temperature in the CMIP SSP245 runs and the large AMOC decline scenario (-12Sv) for Western North America as in Figure 3

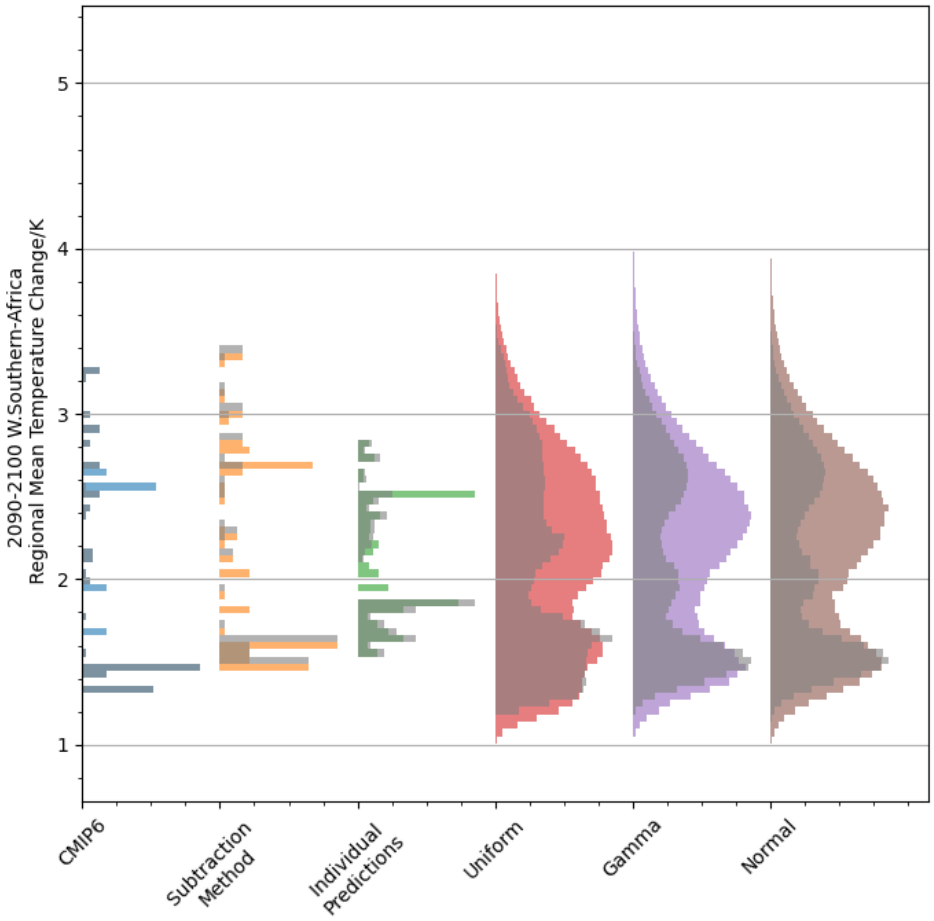


Fig. 72 Histograms of the 2090-2100 regional mean temperature in the CMIP SSP245 runs and the large AMOC decline scenario (-12Sv) for West Southern Africa as in Figure 3

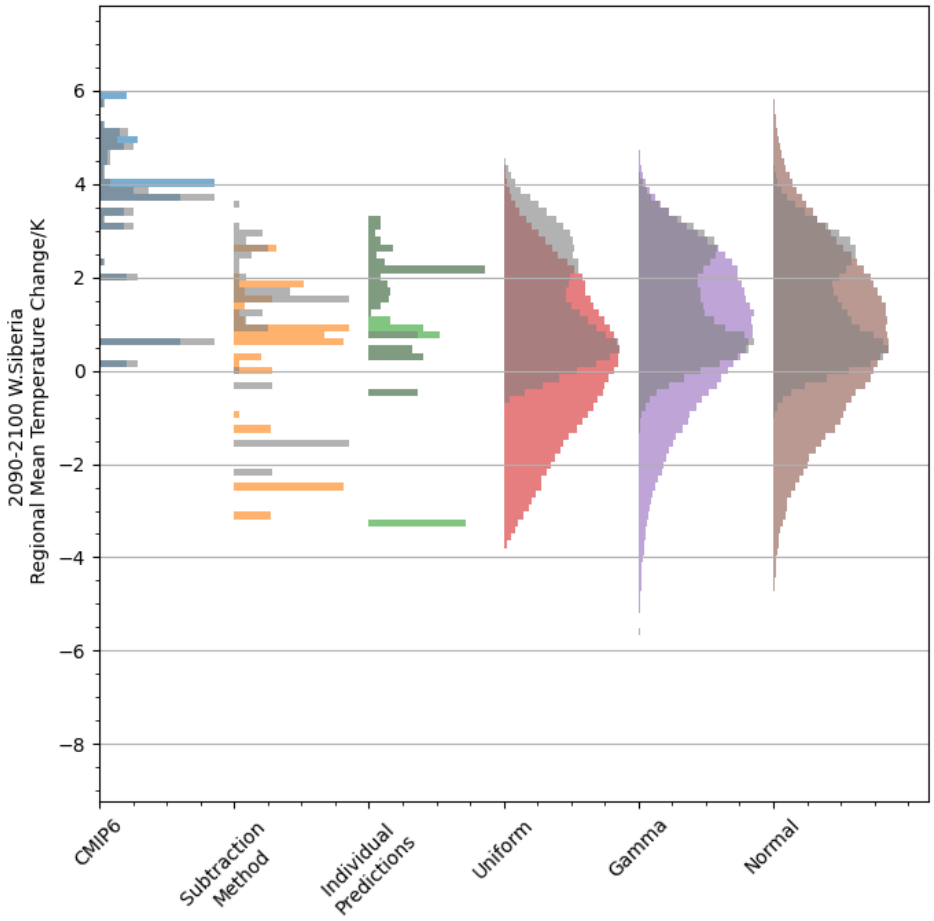


Fig. 73 Histograms of the 2090-2100 regional mean temperature in the CMIP SSP245 runs and the large AMOC decline scenario (-12Sv) for Western Siberia as in Figure 3

References

[1] Swart, N.C., Cole, J.N., Kharin, V.V., Lazare, M., Scinocca, J.F., Gillett, N.P., Anstey, J., Arora, V., Christian, J.R., Hanna, S., *et al.*: The canadian earth system model version 5 (canesm5. 0.3). Geoscientific Model Development **12**(11), 4823–4873 (2019)

[2] Hurrell, J.W., Holland, M.M., Gent, P.R., Ghan, S., Kay, J.E., Kushner, P.J., Lamarque, J.-F., Large, W.G., Lawrence, D., Lindsay, K., *et al.*: The community earth system model: a framework for collaborative research. Bulletin of the American Meteorological Society **94**(9), 1339–1360 (2013)

[3] Danabasoglu, G., Lamarque, J.-F., Bacmeister, J., Bailey, D., DuVivier, A., Edwards, J., Emmons, L., Fasullo, J., Garcia, R., Gettelman, A., *et al.*: The community earth system model version 2 (cesm2). Journal of Advances in Modeling Earth Systems **12**(2), 2019–001916 (2020)

[4] Döscher, R., Acosta, M., Alessandri, A., Anthoni, P., Arneth, A., Arsouze, T., Bergmann, T., Bernadello, R., Bousetta, S., Caron, L.-P., *et al.*: The ec-earth3 earth system model for the climate model intercomparison project 6. Geoscientific Model Development Discussions **2021**, 1–90 (2021)

[5] Williams, K.D., Copsey, D., Blockley, E., Bodas-Salcedo, A., Calvert, D., Comer, R., Davis, P., Graham, T., Hewitt, H., Hill, R., *et al.*: The met office global coupled model 3.0 and 3.1 (gc3. 0 and gc3. 1) configurations. Journal of Advances in Modeling Earth Systems **10**(2), 357–380 (2018)

[6] Boucher, O., Servonnat, J., Albright, A.L., Aumont, O., Balkanski, Y., Bastrikov, V., Bekki, S., Bonnet, R., Bony, S., Bopp, L., *et al.*: Presentation and evaluation of the ipsl-cm6a-lr climate model. Journal of Advances in Modeling Earth Systems **12**(7), 2019–002010 (2020)

[7] Müller, W.A., Jungclaus, J.H., Mauritsen, T., Baehr, J., Bittner, M., Budich, R., Bunzel, F., Esch, M., Ghosh, R., Haak, H., *et al.*: A higher-resolution version of the max planck institute earth system model (mpi-esm1. 2-hr). Journal of Advances in Modeling Earth Systems **10**(7), 1383–1413 (2018)

[8] Mauritsen, T., Bader, J., Becker, T., Behrens, J., Bittner, M., Brokopf, R., Brovkin, V., Claussen, M., Crueger, T., Esch, M., *et al.*: Developments in the mpi-m earth system model version 1.2 (mpi-esm1. 2) and its response to increasing co2. Journal of Advances in Modeling Earth Systems **11**(4), 998–1038 (2019)